Published in partnership with the Australian Regenerative Medicine Institute



https://doi.org/10.1038/s41536-025-00391-5

Systemic factors associated with antler growth promote complete wound healing



Qianqian Guo ^{1,2,4}, Guokun Zhang^{1,4}, Jing Ren¹, Jiping Li¹, Zhen Wang¹, Hengxing Ba¹, Zihao Ye¹, Ying Wang³, Junjun Zheng² ⊗ Chunyi Li ¹ □

Deer antlers are the only mammalian appendages that can fully regenerate from periosteum of pedicles (PP). This regeneration process starts from regenerative healing of wounds. Removal of PP abolishes antler regeneration, however, the regenerative cutaneous wound healing proceeds, indicating that some factors in the circulation contribute to this healing. In this study, we produced a wound in the scalp of deer either in antler regeneration period (ARP) (n = 3) or in non-ARP (n = 3). Results showed full regeneration took place only when the wound was created during ARP. Interestingly, topical application of systemic factors from ARP (n = 9) promoted regenerative wound healing in rats. Comparative proteomics analysis (n = 3) revealed that PRG4 and IGF-1 were high during ARP, and topical application of PRG4 + IGF-1 promoted restoration in rat FTE wounds. We believe that, ultimately, incorporating systemic factors into advanced wound care modalities could offer new opportunities for regenerative healing in the clinical setting.

As the first line of defense against external insults, the skin, the largest body structure, is constantly exposed to injuries. In adult mammals, skin generally develops a fibrotic scar following deep wounding¹. Scars differ from normal skin in that they lack cutaneous appendages, such as hair follicles and glands, and are characterized by fibrotic extracellular matrix (dense and parallel fiber bundles versus a 'basket-weave' pattern in normal skin); thus, they lack a normal thermoregulatory or barrier function^{1,2}.

Despite efforts to reduce scar formation in the clinical setting, we lack effective treatments to obtain a regenerative outcome in wound repair due, in part, to the lack of appropriate animal models that would enable a fuller understanding of the fundamental mechanisms of regenerative wound healing in a natural setting. Although fetal skin in mammals (including humans) exhibits scarless healing^{3,4}, few adult mammals do likewise³. Promising models of scar-free healing include spiny mice (Acomys spp.) and MRL mice, but in both cases, the type of wound healing is fundamentally different from that of adult human skin^{3,5–7}. Therefore, there is a need for a model in a large and tight-skinned adult mammal, where wound healing approximates that of humans and, at the same time, exhibits regenerative repair.

Although complete regeneration of appendages is rare in adult mammals, the deer is an exception in that their antlers are fully regenerated annually from the permanent bony protuberances, known as pedicles^{8,9}. This process initiates from the regenerative wound healing over the apex of a pedicle stump following the casting of the previous (hard) antler¹⁰. Our

previous studies have confirmed that the very rapid healing (within 2 weeks) of this large wound (up to 10 cm diameter) is achieved in a regenerative manner including regeneration of cutaneous appendages, such as hair follicles and sebaceous glands (SGs)¹¹. The regenerated architecture and pattern of the healed skin is velvet-like and markedly different from that of the pedicle skin (typical scalp skin), from which the healed skin originates, thus termed velvet skin or velvet^{10,12–14}. Thus far, the mechanism underlying this unique type of regenerative wound healing with a transition from scalp skin to velvet skin has not been explored.

Full antler regeneration is known to be driven by antler stem cells (AnSCs) resident in the pedicle periosteum (PP) or in the early antler blastema^{15–17}, and starts from almost scarless healing of a cutaneous wound. Recent studies have shown that local paracrine factors from the closely abutted PP, where the AnSCs reside, play a key role in this regenerative healing of pedicle wounds^{11,18,19}. Interestingly, when we investigated the mechanism underlying full antler regeneration, we found that while PP deletion abolishes antler regeneration and the transition to velvet skin, regenerative wound healing over the pedicle stump still takes place although the type of healed skin is essentially no different from that of the pedicle skin²⁰. These results clearly indicate that systemic factors from the circulating blood must be involved in this generic regenerative wound healing, whereas local factors from the PP are indispensable for antler regeneration and for the change in skin type involved in the healing process.

¹Institute of Antler Science and Product Technology, Changchun Sci-Tech University, Changchun, Jilin, China. ²Institute of Special Animal and Plant Sciences, Chinese Academy of Agricultural Sciences, Changchun, Jilin, China. ³CAS Key Laboratory of Tissue Microenvironment and Tumor, Shanghai Institute of Nutrition and Health, University of Chinese Academy of Sciences, Chinese Academy of Sciences, Shanghai, China. ⁴These authors contributed equally: Qianqian Guo, Guokun Zhang. —e-mail: zhengjunjun@caas.cn; lichunyi1959@163.com

To test this hypothesis, we believe that it is necessary to tease apart the effect of systemic factors from local factors, where one approach to achieving this is to shift the site of wound healing to other somatic sites, other than from the apex of the pedicle. In this study, we constructed a full-thickness excisional (FTE) wound model in the forehead region in sika deer to ensure elimination of the effects of local factors. Notably, in a previous study, we castrated male sika deer stags in winter to induce hard antler casting and regeneration of new antler²¹; we found that the rate of wound healing over the pedicle stump was severely impaired, and although regenerative wound healing with velvet skin and antler regeneration were eventually achieved, the quality and quantity of both events were compromised, compared to those that occurred naturally in late spring or early summer (unpublished data). These results indicate that systemic factors in the circulating blood of the stag must be different in composition and in concentration between the two seasons of spring and winter.

To test this assumption, we created the same type of wounds in two different seasons, summer and winter and carefully recorded the process of wound healing both quantitatively and qualitatively. To investigate whether the effective systemic factors for regenerative wound healing were species-specific, we also tested their effects on the healing of dorsal cutaneous wounds in a rat model. We then performed comparative proteomics analysis of the systemic factors from the antler regeneration period (ARP) with the non-regeneration period (non-ARP) to identify the key differentially expressed factors that might effectively promote regenerative wound healing.

Overall, the purpose of our study was to confirm whether the blood-carried systemic factors collected during ARP and non-ARP would produce different wound healing outcomes, i.e., regeneration or scar formation, no matter in deer or rats, and to identify the potentially effective differential factors. We believe that further isolation and identification of the molecules responsible for the full skin regeneration without scar in blood-carried systemic factors collected during ARP would lay the foundation for scarless wound healing in the clinical setting.

Results

Forehead wounds in ARP exhibits regenerative healing in sika deer

Identical cutaneous wounds of 20 mm in diameter in full-thickness skin (Fig. 1a) were created in the forehead region of adult male sika deer during both the antler regenerating (ARP) and non-regenerating periods (non-ARP). On post-operative day (POD) 30 after excisional injury (Fig. 1b), the scab remained in the center of the wounds in non-ARP. In contrast, in the wounds in ARP, scabs had flicked off to reveal that wound healing was morphologically complete. By POD 60 (Fig. 1b), the non-ARP wounds exhibited healing with scarring, having a distinct boundary with the uninjured skin. Whereas, the ARP wounds exhibited almost scarless healing, and the boundary between the wound margin and uninjured skin was barely distinguishable (Fig. 1b).

Histological analysis confirmed the restoration of skin appendages (Fig. 1c and Supplementary Figs. 1 and 2a) with numerous neogenic hair follicles (HFs), SGs, and sweat glands (SWGs). These regenerated skin appendages were also confirmed by the expression of specific cytokeratins 14 and 19 for HF/SG, and cytokeratin 18 for SWG (Fig. 2a and Supplementary Fig. 2b) and positive staining of oil red O for lipid (Fig. 2a). Despite the existence of epithelial invaginations within the healed skin in non-ARP wounds, these structures failed to evolve into definite HFs at least by POD 60 (Fig. 1c and Supplementary Fig. 1). HFs, if any, present in the non-ARP wounds were all limited to the wound margins (Fig. 1c and Supplementary Fig. 1). Quantification of HFs and SGs on POD 60 confirmed that the numbers of HFs and SGs in the ARP wounds were restored to 72% \pm 8.5% and 79% \pm 9.2%, respectively of the pre-injury levels; in contrast, the non-ARP wounds restored only to $12\% \pm 3.2\%$ and $26\% \pm 7.0\%$ (Fig. 2b, c). The fact that there were more regenerated HFs and SGs in the ARP wounds compared with non-ARP wounds may be attributed in part to the presence of more dividing cells in the epidermis (especially the basement membrane)

and dermis (especially HFs and SGs) in the ARP wounds compared with the non-ARP wounds (Fig. 2d, e and Supplementary Fig. 3).

Skin ECM architecture/organization is integral part of the functional skin. Therefore, we evaluated the quality of ECM in healed tissues from ARP- and non-ARP wounds, including the density and architectural arrangement of collagen fibers using unwounded skin as a control. The ARP wounds exhibited more neogenic collagen fibers on POD 9 (Fig. 2g). Collagen fibers, primarily collagen I, densely occupied the wound bed of both ARP- and non-ARP wounds on POD 30. On POD 60, thickened and robust collagen fibers in the ARP wounds, including both collagen I and III, were rearranged through remodeling to a basket-weave-like pattern, resembling that of intact dermis (Fig. 2f, g). In contrast, fine and immature collagen fibers that filled the wound bed of non-ARP wounds were rearranged in a thick parallel bundle fashion with collagen I dominating the healing dermal tissue, reminiscent of a human scar. Taken together, by POD 60, the non-ARP wounds healed with a fibrotic scar, but the ARP wounds showed appendage neogenesis and matrix architecture restoration, indicating a process of regenerative healing.

Molecular hallmarks of differential healing outcomes

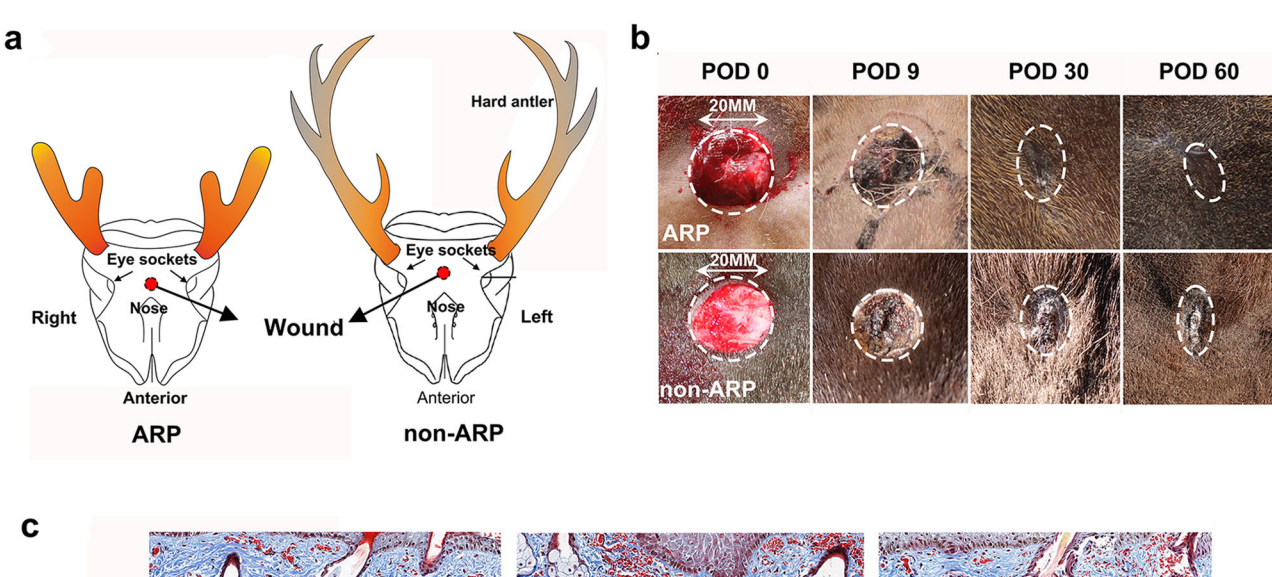
As wound healing comprises multiple phases, it is critical to examine each phase at the cellular and molecular levels. We detected the inflammatory response to wounding in each type of healing using L-Plastin (pan-leukocytic marker)²² staining. In both types of healing, an influx of leukocytes was observed on POD 3 after wounding, and the number of leukocytes increased continually until it peaked on POD 9 (Fig. 3a). Quantitative analysis showed no significant differences in the expression of L-Plastin between the two groups, but the average expression level of L-Plastin in the ARP wounds was lower than that in the non-ARP wounds on POD 3, 9 and 14, respectively (Fig. 3b).

The transition from the fibroblast to the myofibroblast during wound healing plays a critical role in the formation of a fibrotic scar $^{23-25}$; therefore, we sought to detect myofibroblasts using specific marker $\alpha\textsc{-}SMA$ staining. Strong specific staining for myofibroblasts was found in the healing skin of the non-ARP wounds (Fig. 3c), where mean optical density (MOD) values of $\alpha\textsc{-}SMA$ staining were significantly higher than those of the ARP wounds on POD 9 (Fig. 3d). We also detected neogenic blood vessels using $\alpha\textsc{-}SMA$ staining as $\alpha\textsc{-}SMA$ expression is also a marker of the blood vessel wall. The results showed that the neogenic vessels were rich in healing tissue in ARP wounds (Fig. 3c), and the number of the vessels was significantly higher than that in the non-ARP wounds both on POD 9 and on POD 60 (Fig. 3e). We therefore conclude that, at least in part, the ARP wounds healed in a regenerative manner likely achieved through impairment in the inflammatory response, a lower level of myofibroblast differentiation, and an increase in angiogenesis compared with non-ARP wounds.

Blood plasma from ARP in sika deer promotes regenerative wound healing in rats

Our previous studies have shown that the large pedicle wound (10 cm diameter or more) left by casting of the previous hard antler naturally achieves regenerative restoration, realized through a paracrine pathway from the closely abutted AnSCs. However, without the presence of the paracrine factors of AnSCs, cutaneous wounds on the forehead region during ARP also healed in a regenerative manner, despite the fact that this healing was not accompanied by a change in skin type from pedicle skin to antler velvet (skin); this indicates that systemic factors during ARP also play indispensable roles in regenerative healing, although the change in skin type may be caused by local factors.

To determine whether the effects of systemic factors on promoting regenerative healing in deer is species-specific, we topically applied lyophilized deer plasma, collected during both ARP (ARPBP) and non-ARP (non-ARPBP), to acute FTE cutaneous wounds in rats (Fig. 4a). On POD 14, in the ARPBP-treated group, scabs had flicked off which revealed the completion of wound healing morphologically, while in the non-ARPBP-treated group, a small scab still remained in the center of the wound (Fig.



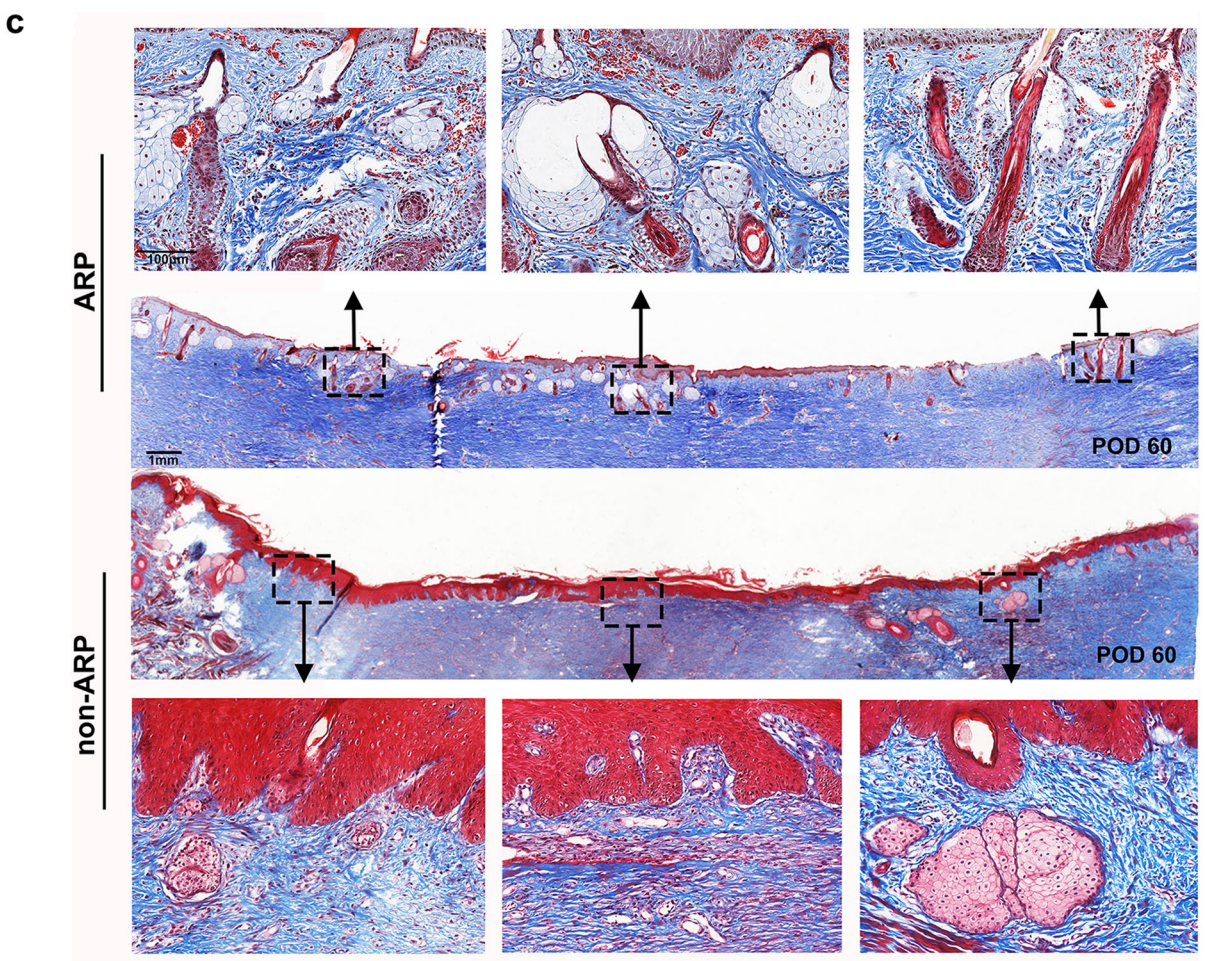
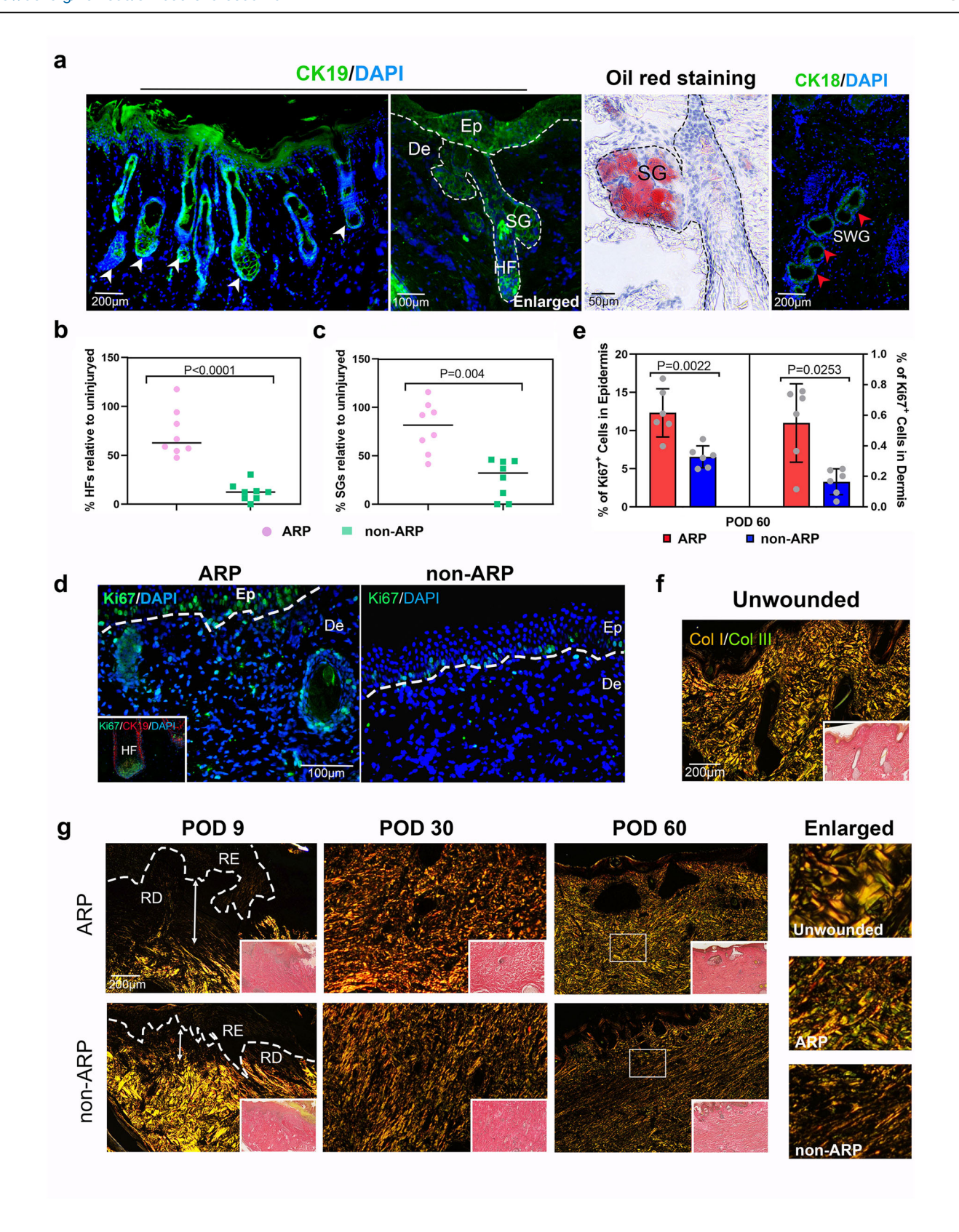


Fig. 1 | Morphological and histological observation during the course of forehead skin healing in adult sika deer in antler regeneration period (ARP) and antler non-regeneration period (non-ARP). a Schematic of wounding sites in ARP and non-ARP. b Full-thickness excision wounds on the foreheads photographed on post-operative day (POD) 0, 9, 30, or 60 days. The healing skin grew centripetally, encircling the scab. Note that at POD 30 after initial wounding, healing was

morphologically completed in the ARP wounds in a regenerative manner, but in non-ARP wounds in a scar manner. **c** Masson's trichrome staining on skin sections from POD 60 ARP and non-ARP excision wounds; note that numerous neogenic appendages were visible in the ARP wounds, but in contrast, significantly fewer appendages were observed in the non-ARP wounds.

4b). On POD 28, a reasonably dense population of hairs was evident on the healed skin of the ARPBP-wound (Fig. 4b), and histological results showed that numerous regenerated skin appendages were distributed in the healing skin; in sharp contrast to the non-ARPBP-treated group, in which very few appendages were seen and only appeared at the wound margin (Fig. 4b–d). These morphologically identified neogenic appendages were further

confirmed to be HFs and SGs, respectively, through CK19 and oil red O staining (Fig. 5a, b). Consistent with the results of HE and Masson's staining, CK19 expression was significantly higher in the ARPBP-treated wounds than in the non-ARPBP-treated wounds. Next, using the expression status of Lef1, a specific marker for neogenic HFs (Fig. 5b and Supplementary Fig. 4), we confirmed the different developmental stages of HFs. The results



showed that the ARPBP-treated wounds had more Lef1⁺ cells than those in the non-ARPBP-treated wounds throughout the healed dermis (Supplementary Fig. 4). Specifically, most Lef1⁺ cells appeared in the bulb region of epithelial invaginations in the ARPBP-treated wounds, suggesting they are the initiation point of HFs regeneration (Fig. 5b). Quantification of the HFs and SGs on POD 28 confirmed that numbers of HFs and SGs were both

significantly higher in the ARPBP-treated wounds (HF: $57\% \pm 6.7\%$, SG: $105\% \pm 12.7\%$) than in the non-ARPBP-treated wounds (HF: $4.4\% \pm 0.71\%$, SG: $14\% \pm 4.7\%$, Fig. 5c, d).

We next detected the proliferating cells in the healing tissues on POD 28 using Ki67 staining. The number of Ki67 $^+$ cells in the epithelial basal layer in the ARPBP-treated wounds was significantly higher than that in the non-

Fig. 2 | Deer forehead skin exhibits regenerative healing after wounding during ARP. a Neogenic HFs, SGs, and SWGs within the ARP wounds stained for Cytokeratin 19 (CK19; green), oil red O (red), and Cytokeratin 18 (CK18; green). Ep, epidermis; De, Dermis; HF, hair follicle; SG, sebaceous gland; SWG, sweat gland. **b, c** Quantification of neogenic HFs and SGs. Note that the numbers of regenerated HFs and SGs in the ARP wounds were significantly higher than that in the non-ARP wounds. Data are shown as the mean \pm SEMs (n=3), with eight fields were randomly chosen from three replicate of each tissue sections for statistical analysis. **d** The diving cells within ARP- and non-ARP wounds stained with Ki67 (green). The inset image shows the proliferating HF cells via staining with Ki67 (green) and CK19 (red). **e** Quantification of diving cells in epidermis and dermis. The number of positive cells was significantly higher in ARP wounds both in epidermis and dermis

compared with non-ARP wounds. Data are shown as the mean \pm SEMs (n=3) with six fields randomly chosen from three replicates of each tissue section for statistical analysis. \mathbf{f} , \mathbf{g} ECM properties for intact skin and ARP- and non-ARP wounds. Col I (red/orange) and Col III fibers (green) were discriminated via picrosirius red staining under polarized light microscope. On POD 9, more collagen fibers were observed in the ARP-wound bed than in the non-ARP wounds. By POD 30, neogenic collagen fibers, mainly collagen I, have filled in the healed tissue of both ARP and non-ARP wounds. Note that on POD 60 in ARP wounds, the collagen fibers were thickened, robust, and rearranged in a basket-weave-like pattern, similar to that of unwounded skin. In contrast, in non-ARP wounds, neogenic collagen fibers were rearranged in a dense parallel bundle fashion, similar to that of fibrotic scar. RD regenerated dermis, RE regenerated epidermis.

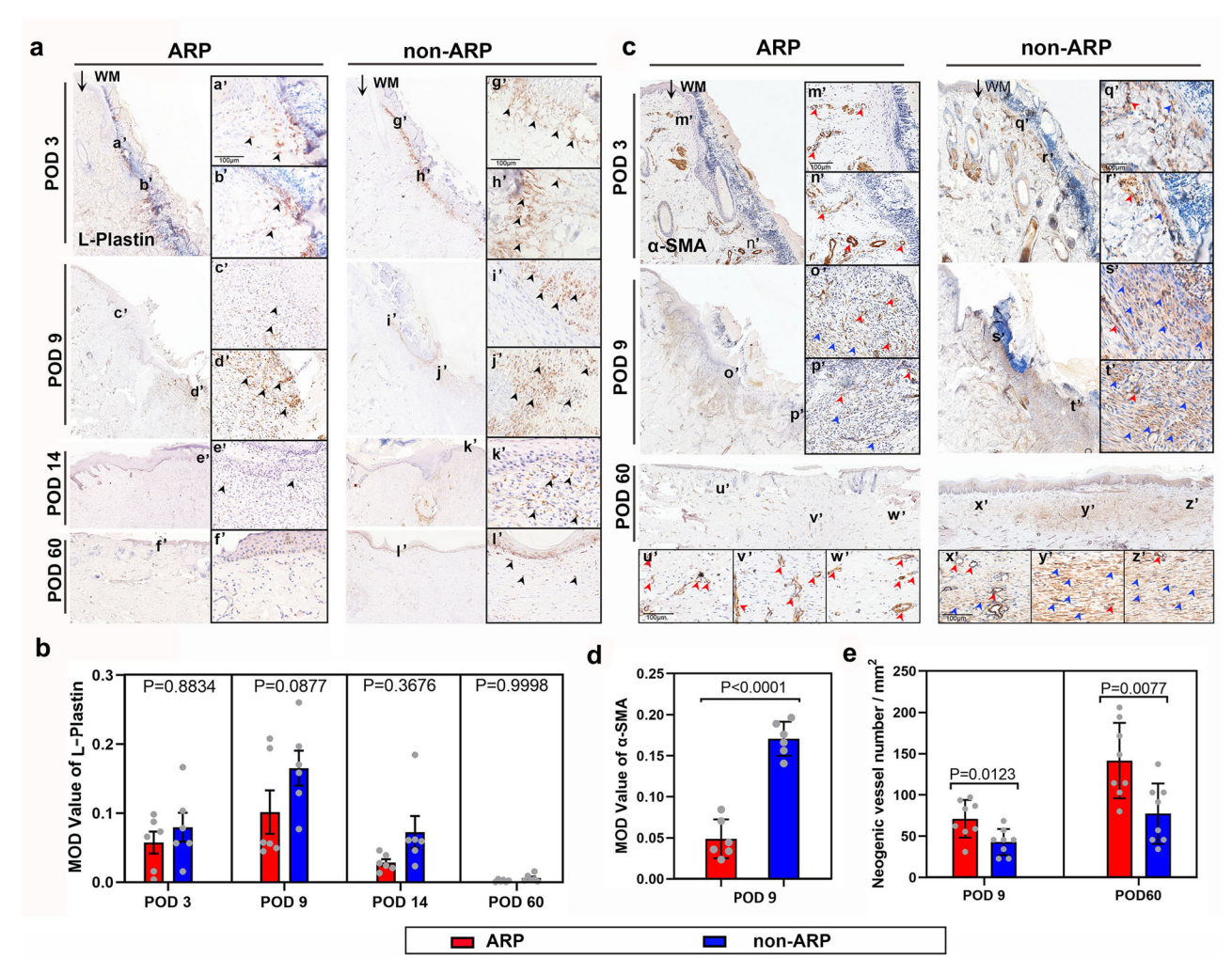


Fig. 3 | Molecular hallmarks during the course of healing of ARP- and non-ARP wounds. a Cells of hemopoietic lineages were detected using L-plastin staining on the wound bed at different time points. An influx of leukocytes (black arrowheads) was observed on POD 3 after wounding in both cases, and the number of leukocytes increased until the peak on POD 9, and then decreased; WM, wound margin. b Quantification of the MOD (mean optical density) value of L-plastin, based on the results of (A). Note that the mean MOD value of L-Plastin staining was increased in ARP wounds compared to non-ARP wounds at any given time point, although the difference was not significant. Data are shown as the mean \pm SEMs (n=3) with six fields randomly chosen from three replicates of each tissue section for statistical analysis. c Myofibroblasts and neogenic blood vessels were detected on the wound bed using α -SMA staining. Strong specific staining for myofibroblasts (blue

arrowheads) was highly significantly detected in the non-ARP wounds compared to the ARP wounds. On the contrary, significantly more neogenic blood vessels (red arrowheads) were observed in the ARP wound bed compared to the non-ARP wounds. **d** Quantification of α -SMA staining for myofibroblasts. Note that the MOD value of α -SMA staining in ARP wounds was significantly higher than that in the ARP wounds on POD 9. Data is shown as the mean \pm SEMs, n=3, six fields were randomly chosen from three replicates of each tissue section for statistical analysis. **e** Quantification of neogenic blood vessels. Note that the number of neogenic blood vessels in ARP wounds was significantly higher than that in non-ARP wounds either on POD 9 or POD 60. Data are shown as the mean \pm SEMs (n=3) with eight fields randomly chosen from three replicates of each tissue section for statistical analysis.

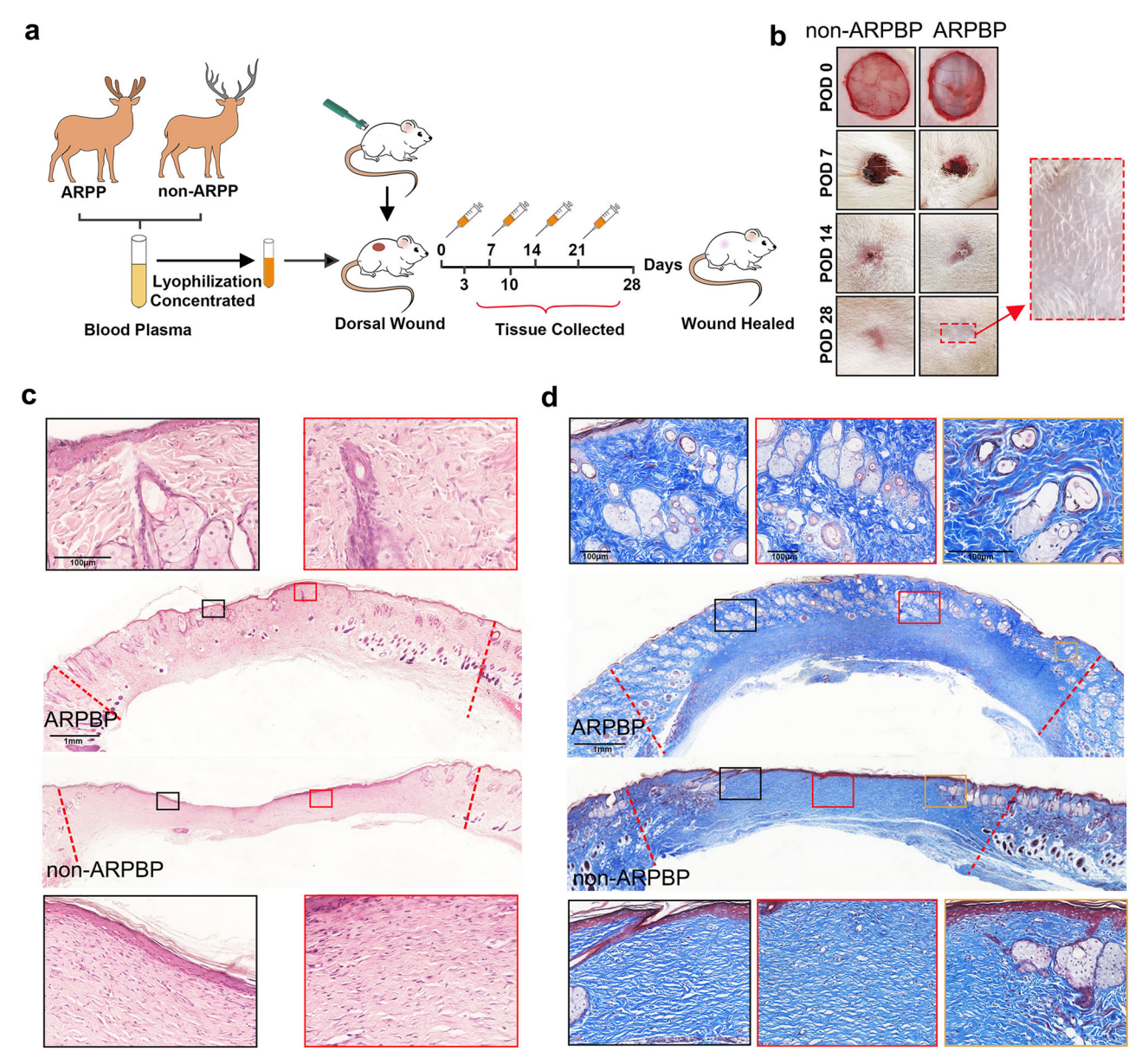


Fig. 4 | Morphological observation and histological assessment of the effects of deer blood plasma from ARP (ARPBP) and non-ARP (non-ARPBP) on cutaneous wound healing. a Schematic diagram of the experimental design.

b Morphological comparison of the healing process of rat dorsal full-thickness wounds between ARPBP and non-ARPBP treatment groups. Note that on POD 28, there is a sparse population of hair in the center of the wound in the ARPBP treatment group. c Skin sections from POD 28 excision wounds with HE staining.

Note that numerous neogenic appendages were observed in the wounds after ARPBP treatment, while very few appendages were seen at the wound margin in the non-ARPBP treatment group. $\bf d$ Skin sections from POD 28 excision wounds with Masson's trichrome staining. Consistent with the HE staining results, ARPBP significantly improved wound healing quality evidenced by restoration of skin appendages.

ARPBP-treated wounds (Fig. 5e, f), suggesting that the increased proliferation rates might be related to further epithelial invagination and transformation into HFs from epithelial invagination in the ARPBP-treated wound epidermis. In the dermis, the number of Ki67⁺ cells in the ARPBP-treated wounds was also significantly higher than in the non-ARPBP wounds and was distributed mainly in the newly forming HFs and SGs (Fig. 5e, g). Overall, treatment with ARPBP promoted the rate of cell proliferation in the healing tissues, which may be related to the formation of HFs and SGs.

To explore the ECM status of the regenerated healing tissue, we measured the density and architectural arrangement of collagen fibers using Sirius red staining. On POD 28 after ARPBP treatment, the pattern of collagen composition and architectural arrangement in the healing dermal tissue were almost restored to the pre-wounding level including both collagen I and III, with a basket-weave-like architecture (Fig. 5h), and the

wound dermis was virtually indistinguishable from the adjacent uninjured dermis, suggesting a complete regeneration of the dermal matrix. In contrast, after the non-ARPBP treatment, the healing tissue comprised predominantly collagen I, which was arranged in a dense parallel bundle fashion, typical of a fibrotic scar. Taken together, our results show that the ARPBP treatment of the acute wounds significantly improved the quality of healing including a completely restored dermis, in contrast to the non-ARPBP treatment, and these effects are not species-specific.

ARPBP inhibits inflammatory and promotes anti-inflammatory response

It has been proposed that whether healing of a wound is realized in a regenerative fashion or as a fibrotic scar is closely associated with the level of inflammatory response, with exaggerated inflammation contributing to

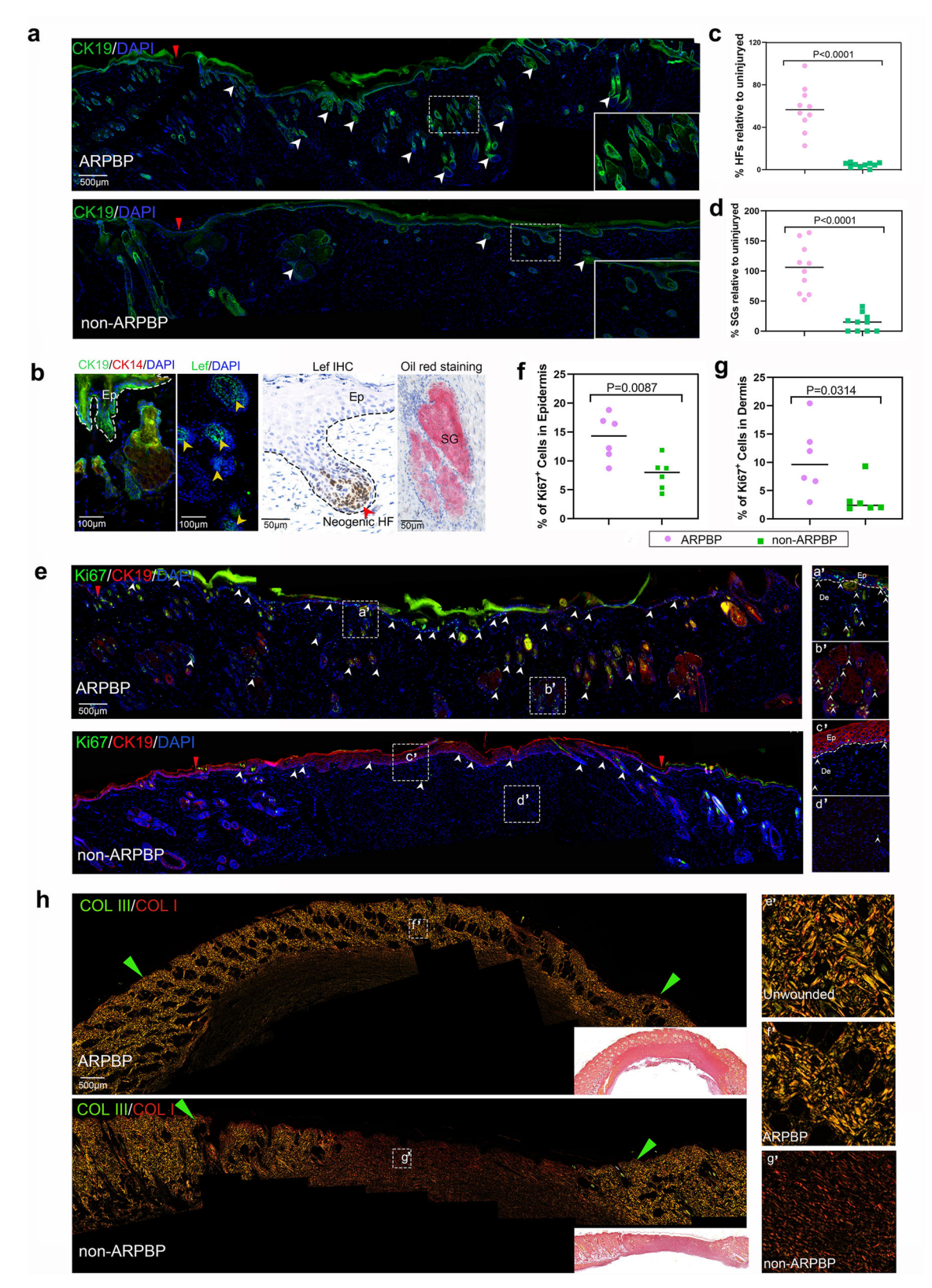


Fig. 5 | ARPBP promotes regenerative wound healing in rats. a, b Neogenic HFs and SGs in the ARPBP-treated wounds, stained with CK19 (green), CK14 (red), Lef1 (green and brown), and oil red O (red). The white arrowheads point to the neogenic HFs and SGs. c, d Quantification of neogenic HFs and SGs. Note that the numbers of regenerated HFs and SGs in the ARPBP treatment group were significantly higher than those in the non-ARPBP treatment group. Data are shown as the mean \pm SEMs (n = 3) with ten fields randomly chosen from three replicates of each tissue section for statistical analysis. e Diving cells in the wound bed stained with Ki67 (green) and

CK19 (red). Note that ARPBP treatment group had significantly more stained cells (white arrowheads) than the non-ARPBP group. \mathbf{f} , \mathbf{g} Quantification of diving cells in epidermis and dermis. Note that the ARPBP group had significantly more ki67 $^+$ cells in both epidermis and dermis than the non-ARPBP group. Data are shown as the mean \pm SEMs (n=3) with six fields randomly chosen from three replicates of each tissue section for statistical analysis. \mathbf{h} ECM ultrastructural properties for healed skin on POD 28. Note that the ECM architecture in the ARPBP group was comparable to normal skin, whereas fibrosis characteristics were evident in the non-ARPBP group.

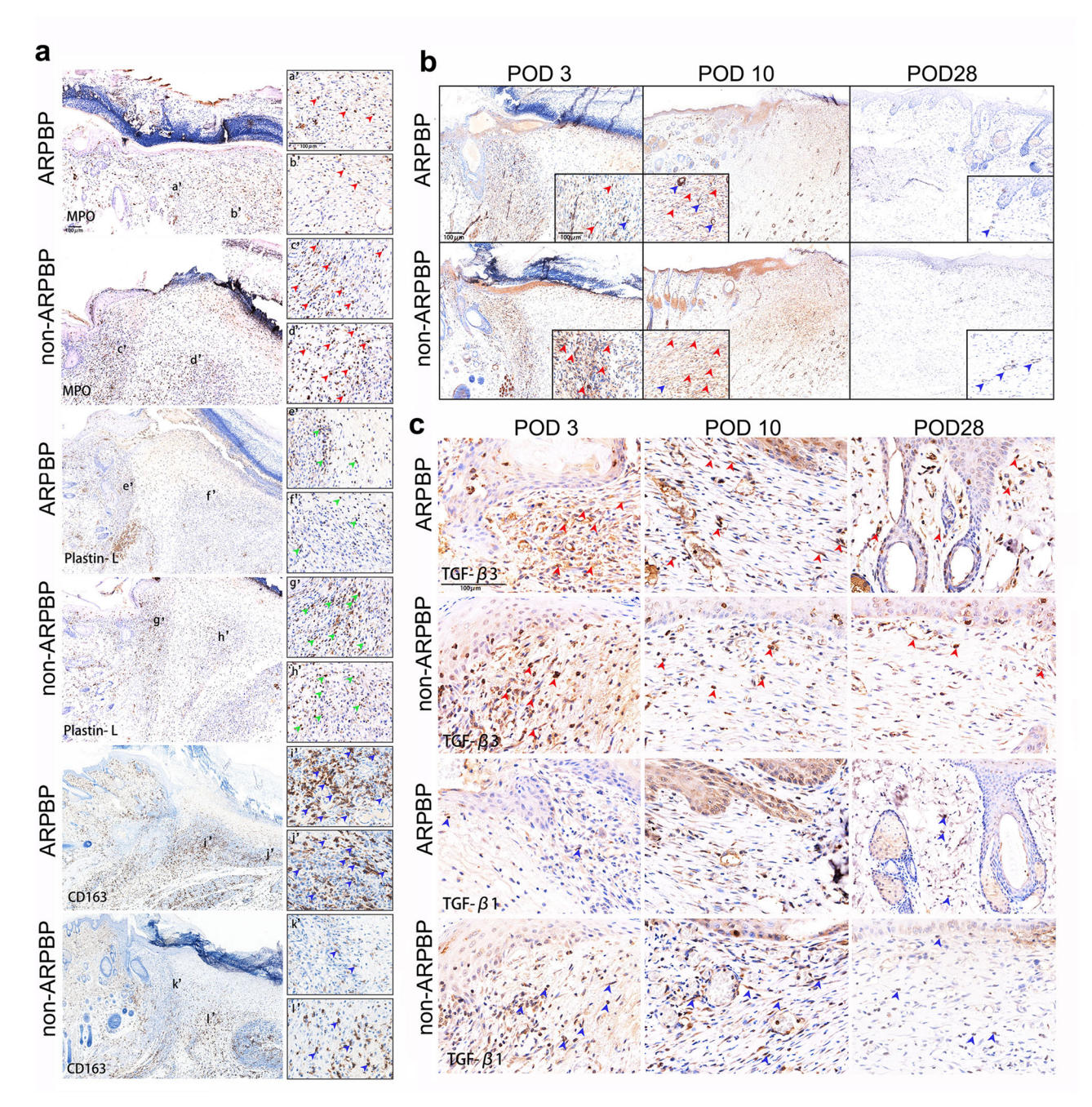


Fig. 6 | Immunohistochemical (IHC) staining. a IHC staining of myeloperoxidase (MPO), L-plastin, and CD163. Note that ARPBP group had much stronger CD163 staining (blue arrowheads), but much weaker staining of MPO (red arrowheads) and L-plastin (green arrowheads). b IHC staining of $\alpha\text{-SMA}$. Note that ARPBP group had much stronger staining for neogenic blood vessels (blue

arrowheads), but much weaker staining for myofibroblasts (red arrowheads), compared to the non-ARPBP group. c IHC staining of TGF- $\beta 1$ and TGF- $\beta 3$. Note that ARPBP group had much stronger TGF- $\beta 3$ (red arrowheads) staining, but much weaker TGF- $\beta 1$ (blue arrowheads) staining, compared to the non-ARPBP group.

increased fibrosis²⁶. In order to characterize the inflammatory response, L-plastin staining was performed on the wound bed on POD 3. Based on the number of L-plastin⁺ cells, we found the non-ARPBP-treated wounds exhibited a more severe infiltration of leukocytes into the wound bed, whereas ARPBP-treated wounds showed weaker positive staining (Fig. 6a). Comparative analysis of L-plastin⁺ cells showed that the number of leukocytes was significantly lower (P < 0.001) in ARPBP-treated wounds than in non-ARPBP-treated wounds (Fig. 7b). To further quantitate the inflammatory response, we examined neutrophil infiltration using staining with myloperoxidase (MPO), a marker of neutrophils. Consistent with the results of L-plastin staining, MPO-staining showed that the number of neutrophils was significantly lower in the ARPBP-treated than in the non-

ARPBP-treated wounds (Figs. 6a and 7a), indicating a reduced inflammatory response after ARPBP treatment. Next, we performed staining with CD163, a marker of anti-inflammatory monocytes, to assess the anti-inflammatory response in the healing tissue on POD 3. The results showed that number of CD163 $^+$ cells in ARPBP-treated wounds was significantly higher than that in non-ARPBP-treated wounds (Figs. 6a and 7c), indicating an enhanced anti-inflammatory response following ARPBP treatment.

ARPBP inhibits myofibroblast differentiation but elevates the ratio of TGF- β 3 to TGF- β 1

Next, we investigated the differences in myofibroblast transition and angiogenesis in the proliferation phase of wound healing in the ARPBP-

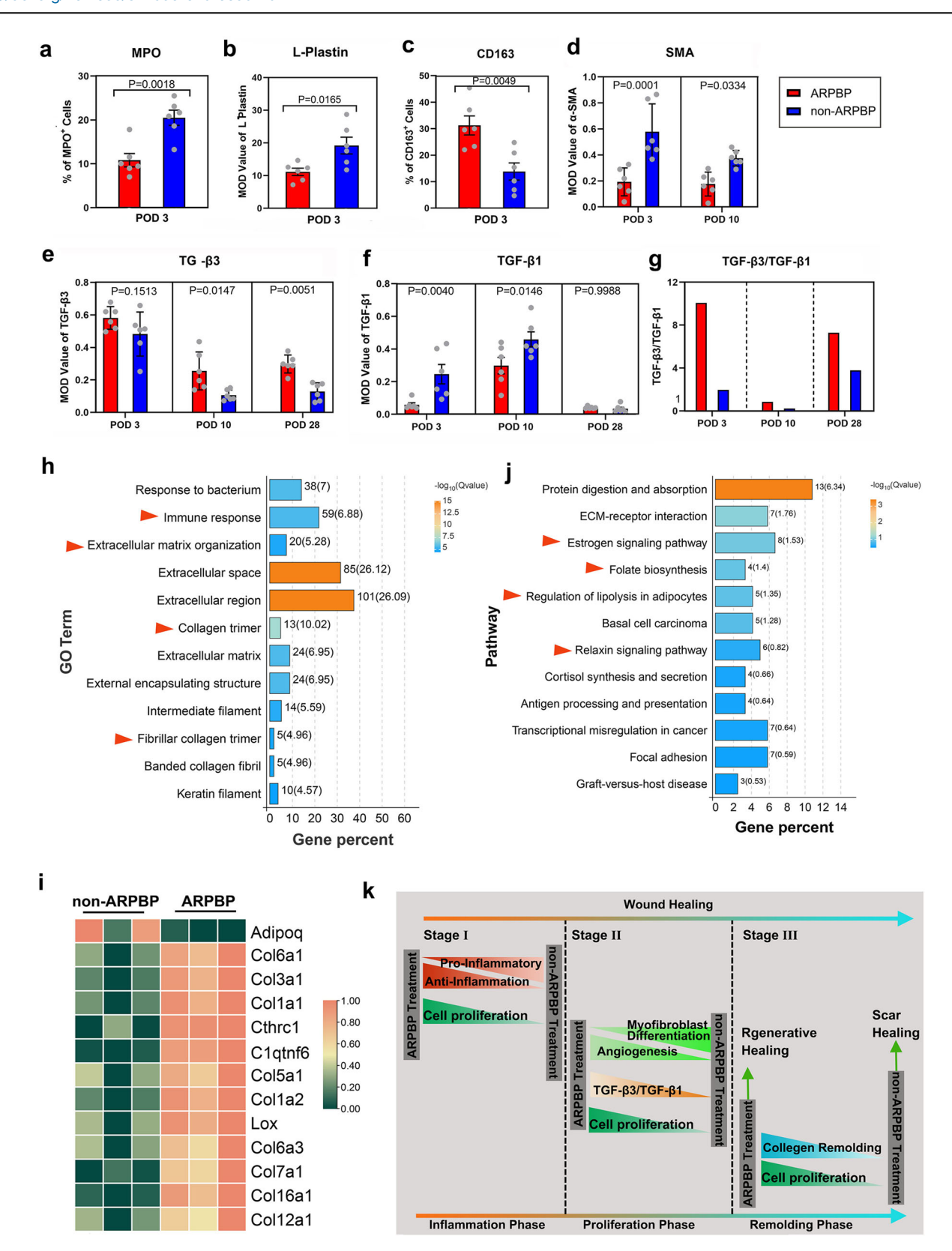


Fig. 7 | Molecular hallmarks during the course of healing in ARPBP- and non-ARPBP-treated wounds. a–f Quantification of the number of MPO $^+$ and CD163 $^+$ cells, and MOD values for L-plastin, α -SMA, TGF- β 1, and TGF- β 3, based on the results of IHC staining. Data are shown as the mean \pm SEMs (n=3) with six fields randomly chosen from three replicates of each tissue section for statistical analysis. g Ratio of TGF- β 3 to TGF- β 1 on POD 3, 10, and 28, calculated as follows: the mean

of TGF- β 3/the mean of TGF- β 1 at each time point. **h, i** RNA-seq comparative analysis of the healed skin tissues sampled on POD 28 between ARPBP- and non-ARPBP-treated wounds. **j** Heatmaps for differential genes enriched in the GO term: collagen trimer. **k** Schematic diagram to depict the major hallmarks of regenerative repair in the ARPBP group compared with the scar repair in the non-ARPBP group.

treated and non-ARPBP-treated wounds using α -SMA staining. Strong positive staining for myofibroblasts was present in the healing tissue in both cases on POD 3. Through the progression of wound healing, the number of myofibroblasts gradually declined to an undetectable level in the healing tissue by POD 28 (Fig. 6b). The intensity of specific staining for myofibroblasts on POD 3 and POD 10 was significantly higher in non-ARPBP-treated wounds than those in ARPBP-treated wounds, respectively (Fig. 7d). In contrast, the newly formed blood vessels were more dense in the ARPBP-treated wounds than those of non-ARPBP-treated wounds.

To further evaluate the differences between the ARPBP-treated and non-ARPBP-treated wounds at the molecular level, we examined the expression levels of genes related to wound healing, namely TGF-β1 and TGF-\beta3 through IHC. Strong TGF-\beta3 expression was detected in the healing tissues of the two types of wounds on POD 3; subsequently, the expression level became low on POD 10, and was maintained a similar level thereafter (Fig. 6c). Comparative analysis showed that the average level of TGF-β3 in the healing tissues of the ARPBP-treated wounds was higher than that of the non-ARPBP-treated wounds, with the differences on POD 10 and 28 being statistically significant (Fig. 7e). Cells positive for TGF-β1 were found only sparsely in the healing tissue of the ARPBP-treated wounds on POD 3, but they increased and peaked on POD 10, subsequently declined to virtually undetectable level by POD 28. The non-ARPBP-treated wounds showed a similar expression trend to the ARPBP-treated wounds, but TGFβ1⁺ cells in the non-ARPBP-treated wounds were significantly higher than in the ARPBP-treated wounds on POD 3 and 10, respectively (Figs. 6c and 7f). Overall, the ARPBP-treated wounds exhibited a higher ratio of TGF-β3 to TGF-β1 than the non-ARPBP-treated wounds (Fig. 7g), a situation reminiscent of fetal regenerative wound healing²⁷.

ARPBP promotes regenerative healing through actively remodeling ECM

The final stage of wound healing is ECM remodeling; dysregulation of ECM remodeling has been shown to contribute to the pathogenesis of several wound healing disorders, such as scar formation. RNA sequencing (RNAseq) analysis of the healing skin from ARPBP-treated and non-ARPBPtreated wounds on POD 28 was performed to gain further insights into the remodeling processes that led to different healing outcomes. GO annotation analysis for differentially expressed genes (DEGs) showed that significantly enriched GO terms were mainly related to ECM architecture/organization through collagen trimer, extracellular matrix organization, extracellular structure organization, intermediate filament, and fibrillar collagen trimer, which were all consistent with the histological results (Fig. 7h). That is, the composition and arrangement of collagen in the ARPBP-treated wounds were comparable to the uninjured levels, in sharp contrast to the parallel arrangement of immature and thin collagen fibers in the non-ARPBP-treated wound. Further, we found that genes for multiple types of collagens were significantly up-regulated in the ARPBP-treated wounds with the enriched term collagen trimer, including fibrillar collagens through Col1a1, Col1a2, Col3a1 and Col5a1 (for structural scaffold formation), and non-fibril forming collagens through Col7a1 (for basement membrane formation), Col6a1 (for beaded-filament forming) and Col12a1 (orchestrating proper skin matrix structure) (Fig. 7i). Kyoto Encyclopedia of Genes and Genomes (KEGG) analysis showed that the significantly enriched pathways for DEGs included the "estrogen signaling pathway" (important in wound healing), "relaxin signaling pathway" (anti-fibrosis and promotion of collagen remodeling²⁸) and several other metabolism-related signaling pathways (Fig. 7j). Taken together, we conclude that it is the ARPBP treatment that has induced ECM regeneration through orchestration of appropriate collagen remodeling.

In summary, wound healing consists of three distinct but overlapping phases (Fig. 7k), effects of ARPBP treatment on regenerative wound healing may be achieved through the impaired inflammatory response, reduced myofibroblast transition, increased angiogenesis, increased ratio of TGF- $\beta 3$ to TGF- $\beta 1$ and orchestrated collagen remodeling; and all these collectively contribute to the final outcome of regenerative wound healing in the ARPBP treatment group compared to the non-ARPBP treatment group.

Regeneration-related factors are enriched in the ARPBP

To identify systemic factors potentially contributing to regenerative healing in either deer forehead wounds or rat dorsal wounds, we performed comparative DIA quantitative proteomics analyses of deer plasma to detect the differentially expressed protein (DEPs) factors between the ARPBP and non-ARPBP. Principal component analysis (PCA) was carried out to determine the spatial distribution, and similarities and differences between the two types of plasma; the results showed that samples collected from the same season were unambiguously grouped together (Fig. 8a). Proteomic results showed that 106 significantly DEPs were enriched and 52 proteins were upregulated, and 54 proteins were down-regulated in the ARPBP compared to the non-ARPBP (Fig. 8b). These DEPs could be divided into 15 subgroups according to their functional classification using PantherDB (Fig. 8c), among which upregulated proteins function as transfer/carrier protein, protein modifying enzyme, etc (Fig. 8d). KEGG analysis showed that DEPs that were significantly enriched in the pathways related to metabolism, including "Cholesterol metabolism", "Proteasome", and "Pyruvate metabolism"; in addition, the platelet activation pathway, which is widely recognized as having a critical role in tissue regeneration^{29,30}, was also enriched (Supplementary Fig. 5).

Given that ARPBP promoted complete regenerative healing and was associated with orderly changes in inflammatory response, cell proliferation, myofibroblast transformation, and matrix remodeling, we focused on the protein factors involved in these processes in the upregulated proteins and identified ten candidate factors that are correlated with wound healing and tissue regeneration, including IGF-1, PRG4, MMP2, POSTEN, ADIPOQ, FMOD, COL12A1, LUM, THBS4, PRL (Table 1). Together, these data suggest that these differentially expressed and wound healing-associated proteins may be the key factors in inducing different healing outcomes.

The combination of PRG4 and IGF-1 on the promotion of regenerative wound healing in rats

Among the above candidate factors, we noted that IGF-1 and PRG4 are involved in multiple wound-healing processes. Consistent with a previous report that IGF-1 is significantly elevated during ARP relative to the other phases of the antler growth cycle and exhibits a strong positive correlation with antler growth rate, we found that plasma levels of IGF-1 during ARP were significantly higher than that during non-ARP; the same was to PRG4. PRG4 was reported capable of enhancing tissue regeneration. To identify the key plasma factors and potential combinations for promoting regenerative wound healing in both deer and rat skin, we focused on these two upregulated factors: IGF-1 and PRG4. The morphological results showed that on POD 14, wounds in the IGF-1 and IGF-1 + PRG4 groups were essentially closed; whereas in the control group, the wounds were still evident (Fig. 9a). Wound closure was significantly accelerated in the IGF-1 or IGF-1 + PRG4 group compared with the control group. Notably, the differences between IGF-1 and IGF-1 + PRG4 groups were also evident on POD 3 and POD 10 with the IGF-1 + PRG4 treatment being the most effective treatment for accelerating wound healing (Fig. 9b). On POD 28, healed skin was harvested for histological evaluation of the quality of healing. The results showed that the healing tissue of control wounds contained dense, parallel collagen bundles without appendages, whereas healing tissues of wounds treated with IGF-1 or IGF-1 + PRG4 demonstrated reduced fibrosis with an appreciable number of HF/SG-like structures appearing at the margin and middle of the wounds (Fig. 9c-e), indicating that PRG4 and IGF-1 are both effective in promoting regenerative wound healing. Notably, the combination of PRG4 and IGF-1 achieved even better results: it accelerated both the rate of wound healing and promoted regenerative wound healing, suggesting that PRG4 and IGF-1 may have additive effects in promoting regenerative wound healing.

Given the role of IGF-1 and PRG4 on angiogenesis, we examined neovascularization on the wound bed to explore the possible paths whereby IGF-1 and PRG4 promote wound healing, using CD31 immunohistochemical staining. The results showed that the neogenic vessels were rich in healing tissue in IGF-1 + PRG4 treated group (Fig. 9f), and the number of

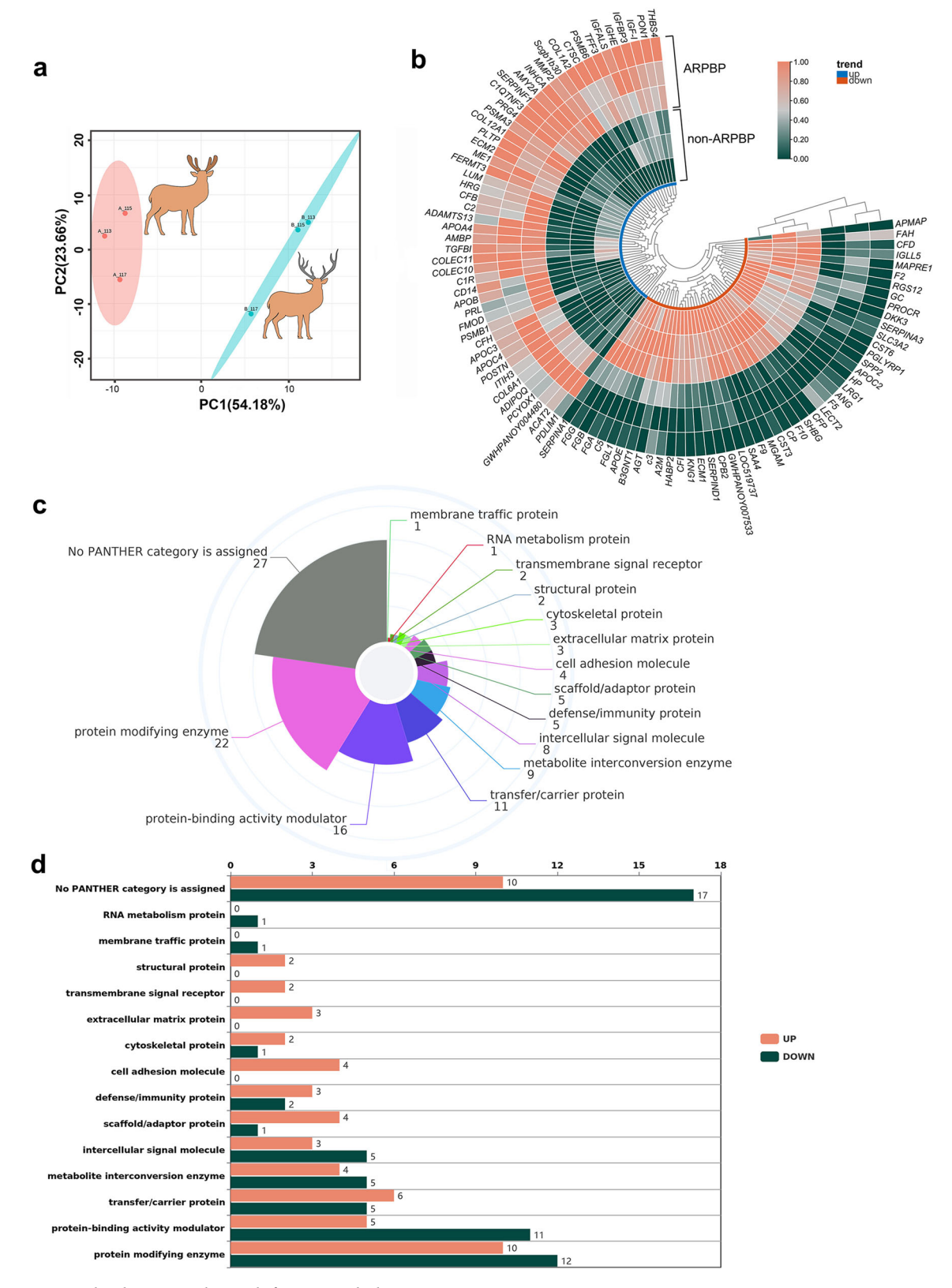


Fig. 8 | Regeneration-related protein/polypeptide factors enriched in ARPBP. a Principal component analysis (PCA) for ARPBP and non-ARPBP samples. Note that the two groups are clearly separated. b Heatmap of differential protein factors in ARPBP contrasted to non-ARPBP. In the innermost circle, blue is for upregulated

proteins, and red is for downregulated proteins. **c** The functional classification of DEPs and distribution of each functional category. **d** Numbers of DEPs including down-regulated (Down) and up-regulated (Up) proteins in each functional category.

Table 1	Table 1 Function of 10 candidate factors in wound healing	s in wound healing		
Protein	Description	Functions in wound healing	In vivo/vitro model	Functional period of wound healing
POSTN	Periostin	Promotes cell proliferation, myofibroblast differentiation, and/or collagen fibrillogenesis ^{44,55}	POSTN-/- mice; Hypertrophic scar fibroblasts	Stage II/II
FMOD	Fibromodulin	Restores scarless healing in late-gestation rat fetal wounds by promoting dermal appendage restoration and organized collagen architectures so reduces scar formation, promotes angiogenesis.	Fetal rat; FMOD-/- mice	Stage II/III
COL12A1	Collagen type XII alpha 1 chain	Regulates fibrillogenesis, CD68 cell lineage infiltration, and myofibroblast survival ²⁹ ; assists in orchestrating proper skin matrix structure, controls growth factor availability and regulates cellular composition and function ²⁸	COL12A1-/- mice; COL12-OE mice	Stage II/III
ADIPOQ	Adiponectin, C1Q, and collagen domain containing	Promots keratinocyte proliferation and migration $^{\circ\circ}_{\circ}$; regulats proliferation, wound repair and apoptosis $^{\circ\circ}_{\circ}$	Adiponectin—/— mice and diabetic mice; Human bronchial epithelial cell lines	Stage I/II
PRG4	Proteoglycan 4	Inhibits the fibrotic response, increases angiogenesis/blood flow to the injury; increases cell proliferation, modulates the immune cell response and mobilizes mesenchymal progenitor cells*°; decreases molecular markers of fibrosis and improved re-vascularization*	Mice; Pig	Stage I/II/III
ГОМ	Lumican	Promotes skin wound healing by facilitating wound fibroblast activation and contraction ⁶⁰ ; plays Mice; LUM—/— mice pivotal roles in skin collagen fibrillogenesis ⁶¹	Mice; LUM-/- mice	Stage II/III
IGF-1	Insulin-like growth factor 1	Dampens the local inflammatory response and promotes re-epithelialization $^{\circ\circ}$; improves the healing speed, promotes cell proliferation and capillaries formation $^{\circ\circ}$	The ovariectomized (Ovx) mice; Diabetic SD rats	Stage I/II/III
HRG	Histidine rich glycoprotein	Plays a role as both an anticoagulant and an antifibrinolytic modifier $^{\mathbb{F}^4}$	HRG-/- mice	Stage I
THBS4	Thrombospondin 4	Promotes fibroblast migration and keratinocyte proliferation ⁶⁶	Mice	Stage I/II
PRL	Prolactin	Controls excessive re-epithelialisation ⁶⁶	Keratinocytes	Stage I/II

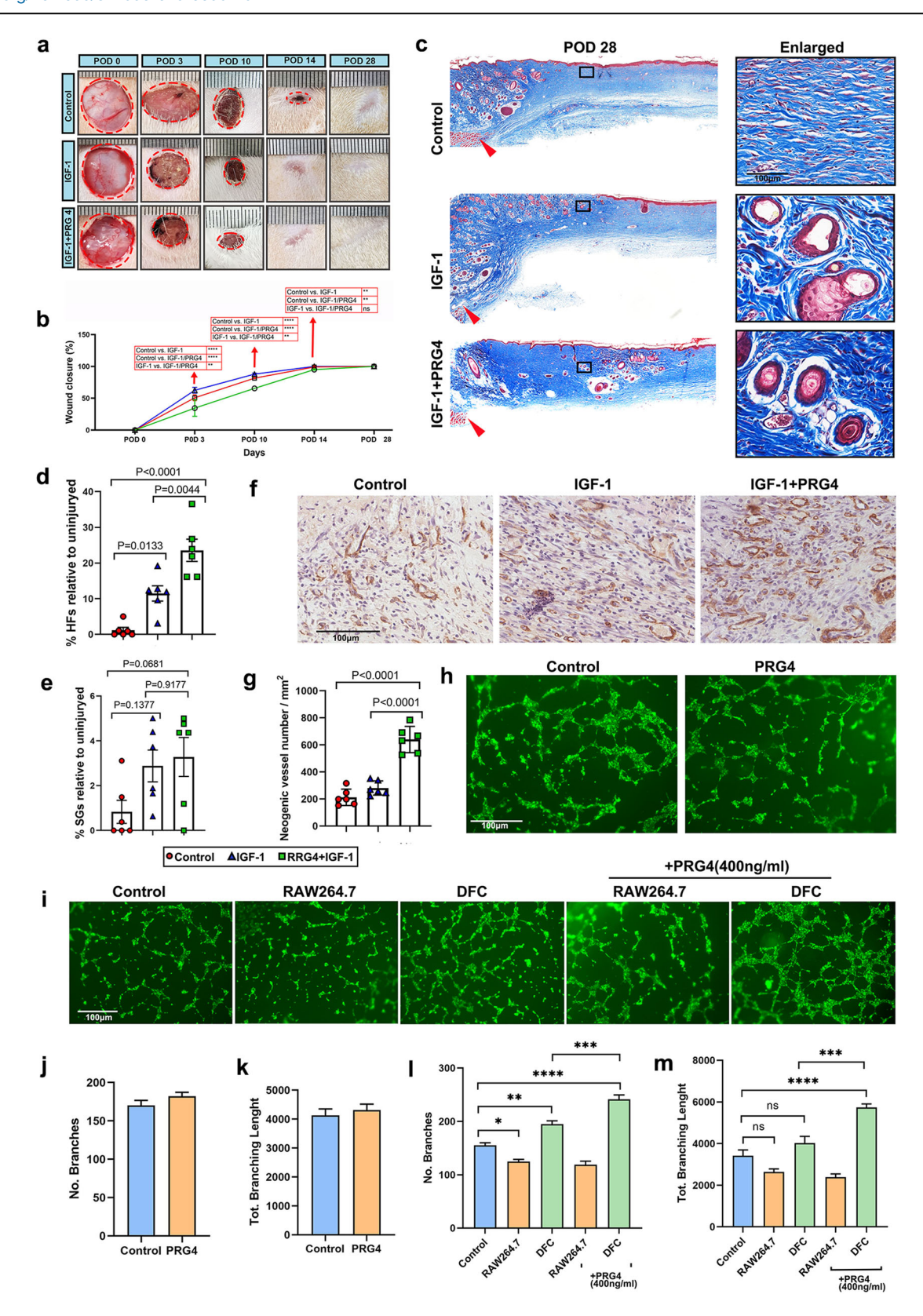
the vessels was significantly higher than in the other groups (Fig. 9g). However, there was no significant difference between the IGF-1 and the control group, suggesting that PRG4 may play a major role in promoting angiogenesis rather than IGF-1.

To test the above hypothesis, a tube formation assay was performed to detect the effect of exogenous PRG4 on angiogenesis in vitro. Unexpectedly, there was no significant difference in vitro angiogenic ability of HUVECs between PRG4 and the control group (its corresponding vehicle control, i.e., PBS, Fig. 9h, j, k). We speculate that PRG4 may not act directly on HUVECs for the promotion of angiogenesis. To confirm this, rat dermal fibroblasts (DFCs) and macrophage RAW264.7 cell lines were respectively co-cultured with HUVECs, and PRG4 was added to explore its indirect effects on the proliferation of HUVECs. As shown in Fig. 9i, the angiogenic ability of HUVECs was significantly increased when being co-cultured with DFCs; whereas angiogenic ability was significantly decreased after co-culture with raw264.7 cells. The addition of PRG4 enhanced the angiogenic effect of DFCs on HUVECs. A large number of intact polygons formed by HUVECs was observed in the DFC + PRG4 group, and quantitative results showed that both branch number and total branch length were significantly increased than other groups (Fig. 9i, l, m), indicating that PRG4 may promote angiogenesis in wound healing by regulating the behavior of DFCs such as the secretion of angiogenesis-related factors such as VEGF, which then functions on endothelial cells.

Discussion

To the best of our knowledge, this is the first detailed study solely focused on the roles of systemic factors from the circulating blood of male deer in regenerative healing of cutaneous wounds applying an approach that can effectively tease apart systemic and local factors. The results, using the creation of FTE wounds on the deer forehead region, exhibited differential healing outcomes depending on whether the healing process took place during the ARP (spring-summer) or in non-ARP (winter). Forehead wounds during ARP achieved regenerative healing, whereas, during non-ARP, scarring was the final outcome. Therefore, key systemic factors from the circulating blood plasma during ARP (ARPBP) must be responsible for the effects. Topical application of ARPBP (as a source of systemic factors) on FTE wounds in the rat promoted healing in a regenerative manner, whereas plasma collected in the non-ARP (non-ARPBP) did not, suggesting that these factors are not species-specific. Our investigations revealed that regenerative healing was achieved through an increase in cell proliferation and angiogenesis, an impairment of the inflammatory response, a reduction in myofibroblast transformation, and an orchestrated remodeling of collagen associated with an increase in the ratio of TGF-β3 to TGF-β1. Comparative proteomics analysis of the ARPBP and non-ARPBP identified some highly up-regulated factors from the ARPBP with regenerationstimulating potential, such as PRG4 and IGF-1. Topical application of IGF-1 or PRG4 + IGF-1 on rat FTE wounds greatly promoted regenerative healing, and the effects of the latter were better than the former. Further analysis confirmed that PRG4 promoted angiogenesis by indirectly regulating endothelial cells via functioning on DFCs, evidenced by the results from our co-culture system. Overall, our findings demonstrate that, although both local paracrine factors and systemic factors during ARP are required for the realization of full antler regeneration, the latter likely creates a unique niche that favors cutaneous regeneration over scar formation after wounding, not only in deer but also in other mammals, such as rats. In contrast, local factors may play a specific role in ARP se, and in alteration of the type of skin.

Deer antlers are the only mammalian structures, that, once lost can fully regenerate¹², and antler regeneration starts from the regenerative healing of a wound (up to 10 cm in diameter) over a pedicle stump^{10,11,20}. Although being claimed as regenerative, the healed skin is no longer a scalp/pedicle-type in nature but rather a velvet-like type, which features a shiny surface with sparsely adorned thin HFs, exaggerated SGs, and absence of SWGs and arrector pili muscle^{10,11}. Interestingly, we found that deletion of the periosteum from a pedicle (which removes local factors) in summer can



effectively abolish antler regeneration but cannot inhibit regenerative wound healing over the periosteum-deprived-pedicle, even though the healed skin was no longer velvet-type, but remained as of scalp/pedicle-type²⁰. This indicates that systemic factors in the circulating blood during the antler growth season must have contributed to the regenerative healing of cutaneous wounds on pedicles; in contrast, local factors from the periosteum

(where AnSCs reside) must be indispensable for antler regeneration, and also noting their involvement in the formation of exaggerated SGs, the lack of SWGs and arrector pili muscle, and in the miniaturization and thinning of HFs. The claim that it is local factors from the AnSCs that change the skin type to velvet-like during wound healing on the pedicle stump is indirectly supported by our recent publications on cutaneous wound healing of rats

Fig. 9 | The effects of PRG4 and IGF-1 on promotion of regenerative wound healing in rats. a Morphological comparison of the healing process of rat dorsal full-thickness wounds between different treatments. b Quantitative evaluation of wound closure during healing (n = 3). Note: application of IGF-1 and/or IGF-1 + PRG4 promoted the rate of wound healing rate compared to the control. The best treatments was that of IGF-1 + PRG4. c Skin sections from the excision wounds on POD 28 with Masson' trichrome staining. Note that HF/SG-like structures were clearly seen at the margin and middle of the wounds in IGF-1 or IGF-1 + PRG4 group, while no appendages were observed in the wound bed of the control group. d, e Quantification of neogenic HFs and SGs. Note that numbers of regenerated HFs and SGs in the IGF-1 and IGF-1 + PRG4 treatment group were significantly higher than those in the control group. Data is shown as the mean \pm SEMs (n = 3) with six

fields randomly chosen from three replicates of each tissue section for statistical analysis. **f** IHC staining of CD31 on POD 10. Note that a large number of neogenic vessels were seen on the wound bed after IGF-1 + PRG4 treatment. **g** Quantification of neogenic vessels. Note that the number of the vessels in IGF-1 + PRG4 group was significantly higher than the other groups, and there was no significant difference between the IGF-1 and the control group. Data is shown as the mean \pm SEMs (n=3) with six fields randomly chosen from three replicates of each tissue section for statistical analysis. **h**, **i** Tube structure on Matrigel could be observed 4 h after seeding HUVECs. **j-m** Quantification of the branch number and the total branch length. Data is shown as the mean \pm SEMs (n=3) with six fields randomly chosen from three replicates for statistical analysis.

using either AnSCs³¹, AnSCs-exosomes²⁵, or AnSCs-conditioned medium³². The treatments in these studies all achieved regenerative wound healing in rats, but without exception, each type of regenerated skin tissue featured at least the partial feature of velvet skin, including partially exaggerated SGs.

Over the years of working with deer, we have observed that cutaneous wounds in male deer, either accidental or resulting from surgery, can heal not only quickly but also in a regenerative manner during spring-summer (the antler growth period), but such healing appears to be slower in winter, and seems more likely to heal with a scar. This observation is now supported by our experimental results, in that the rate of healing of the pedicle wound in winter, induced by castration, was less than half of that in summer, and notably the quality of healing was also inferior (unpublished data). Therefore, we hypothesized that systemic factors in ARPBP must contain key factors that support regenerative wound healing compared with non-ARPBP. To verify this assumption in the present study, we created FTE wounds on the deer forehead regions both in summer and in winter, and the results convincingly demonstrated that wounds in summer healed in a regenerative manner, whereas in winter the wounds healed in a scarring manner. Next, we respectively collected ARPBP and non-ARPBP, for the treatment of acute wounds in a FET model in rats and found that the former significantly improved the quality of wound healing and promoted skin regeneration, while the latter did not. Taken together, the above results confirmed that systemic factors in ARPBP could support the robust regeneration of skin tissues after wounding and are not species-specific.

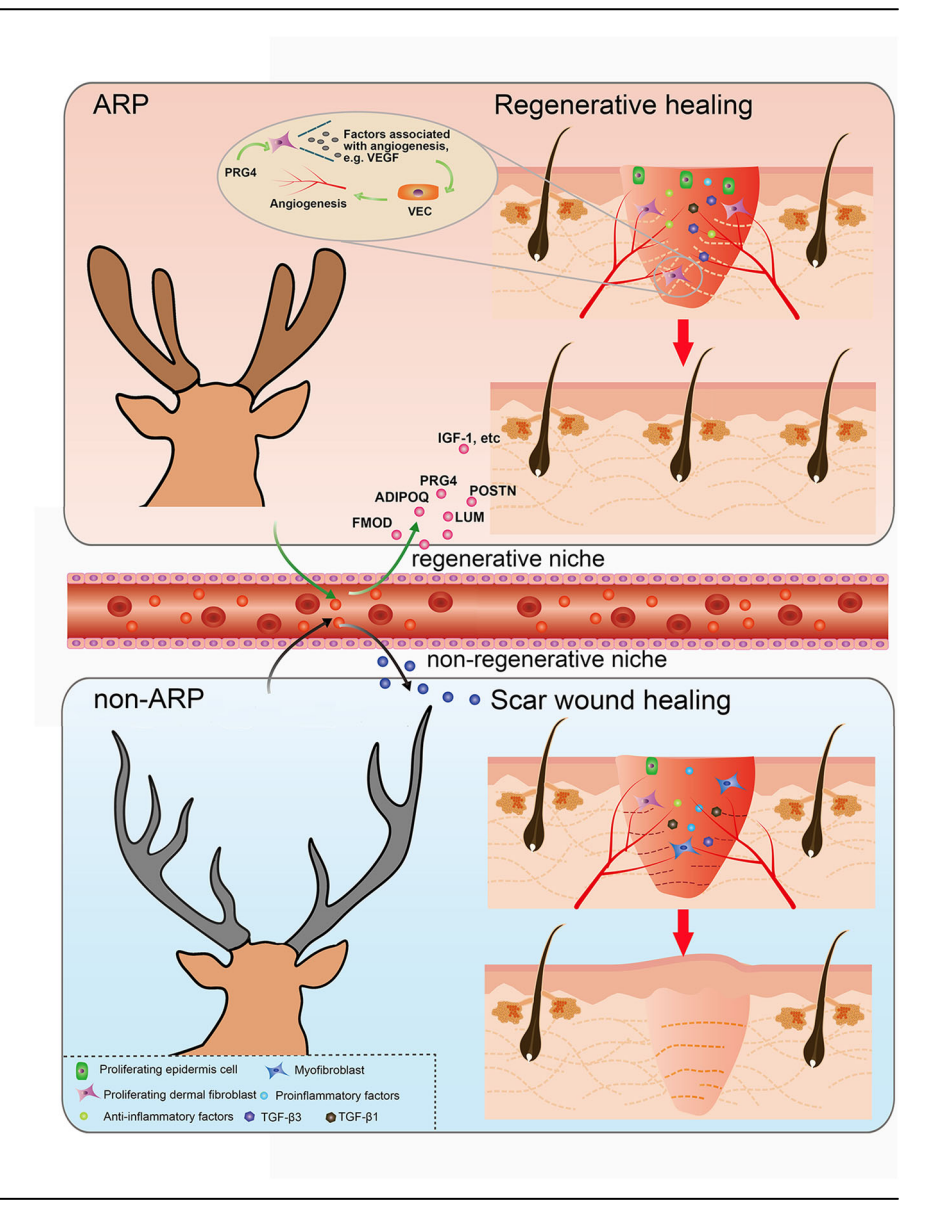
Wound healing is generally divided into three distinct but overlapping phases: inflammation, proliferation, and remodeling 33 . To identify the underlying mechanism of a regenerative path induced by systemic factors in ARPBP, the major hallmarks of healing in these three phases were investigated. In the inflammation phase, ARPBP treatment promoted an anti-inflammatory but suppressed a pro-inflammatory response; in the proliferation phase, ARPBP inhibited myofibroblast differentiation, but increased angiogenesis and the ratio of TGF- β 3 to TGF- β 1; in the remodeling phase, ARPBP induced ECM regeneration through orchestrated collagen remodeling (Fig. 10). These results indicate that the systemic factors functioned in the above unique molecular events may be the key factors for promoting regenerative wound healing.

To identify the putative factors in deer blood plasma collected in the summer, we conducted a comparative analysis through DIA quantitative proteomics between ARPBP and non-ARPBP. The results showed that the differentially up-regulated proteins in ARPBP were mostly related to wound healing or tissue regeneration, and from which we identified ten candidate factors, including IGF-1, PRG4, POSTN, ADIPOQ, FMOD, etc. The plasma levels of IGF-1 have long been reported to be significantly elevated during the antler growth phase relative to the other phases and show a strong positive correlation with the rate of antler growth^{29,34-36}. It is known that IGF-1 is a potent mitogen and plays an important role in increasing the proliferation of mesenchymal stem cells and chondrocytes resident in the tip of growing antlers³⁷⁻⁴⁰, indicating that its high-level expression likely contributes to the enhanced effects on cell proliferation in the healing tissues both in deer or in the rat as shown in the present study. Here, we examined the effect of IGF-1 on wound healing in rats and found that it significantly improved wound healing, including faster healing speed and increased healing quality. More surprisingly, the combined application of both IGF-1 and PRG4 (proteoglycan 4) showed a better therapeutic effect than that of IGF-1 alone. PRG4 is a boundary lubricant originally identified in articular cartilage and has been since shown to have immunomodulation and antifibrotic properties^{41,42}. Recent reports have shown that PRG4 treatment could improve repair quality by increasing re-vascularization after fullthickness skin wounds in a preclinical porcine model⁴³. IGF-1 has also been reported to play a role in angiogenesis, so CD31 staining was performed to determine whether the combined application of PRG4 and IGF-1 would improve wound healing by promoting angiogenesis. Surprisingly, IGF-1 had no significant effect on the promotion of neovascularization, while the combination of IGF-1 and PRG4 significantly increased neovascularization, suggesting that PRG4 plays a major role in promoting re-vascularization rather than IGF-1. Subsequent in vitro experiments confirmed that PRG4 indirectly enhanced the ability of tubing formation by HUVECs via regulating DFCs, which may be achieved by increasing the expression of angiogenic-related growth factors, such as VEGF. This assumption requires further verification experimentally. In addition to IGF-1 and PRG4, other differential candidates up-regulated in ARPBP have also been reported to contribute to tissue regeneration through functioning in different stages of wound healing. For example, POSTN appears to be important for stimulating keratinocyte proliferation and collagen fibrillogenesis⁴⁴, ADIPOQ regulates cutaneous wound healing by promoting keratinocyte proliferation and migration⁴⁵. In addition, the sources of the highly contained factors in the ARPBP warrant also further exploration. Amongst these sources, AnSCs resident in PP, which drives the whole antler regeneration during ARP⁴⁶, would be an unneglected one. Whether the putative factors of the AnSCsderivative are regenerative wound healing-promoting is worthy of further exploration.

Taken together, ARPBP treatment could achieve regenerative healing, but non-ARPBP could not, in which differential systemic factors must play crucial roles. Furthermore, our finding may go even beyond the cutaneous wound healing, for instance, our ARPBP may also functions on bone fracture and internal parts of an open injury, if that is the case that would make our finding even more significant. In summary, regenerative wound healing over a pedicle stump prior to antler regeneration is regulated by both local and systemic factors. Local factors play indispensable roles in ARP se and in the alteration of the type of healing skin (to velvet skin), which includes miniaturization of HFs, production of large and multi-lobed SGs, and terminating the appearance of SWGs and arrector pili muscle. In contrast, systemic factors promote generic wound healing including enhancing the anti-inflammatory, suppressing the pro-inflammatory response, increasing angiogenesis, inhibiting myofibroblast transition, increasing the ratio of TGF-β3 to TGF-β1, and orchestrating collagen remodeling. These findings are highly likely to have potential medical applications: (1) through analysis of systemic factors, we may identify molecules/substances specifically responsible for the regulation of the formation of each type of skin appendages, such as HFs, SGs, and SWGs; (2) to find and isolate the molecules responsible for the full regeneration of skin without scar, in order to design a synthetic medicine that could be used to both reduce the time of recovery from surgery and injury, as well as to induce full regeneration of skin in those cases without the unesthetic scars.

Fig. 10 | Schematic illustration depicts the different healing outcomes in the forehead region under the influence of systemic factors either from circulating blood in ARP or non-ARP in sika deer.

ARP Antler regeneration period, non-ARP non-Antler regeneration period. Created with Adobe Illustrator and Adobe Photoshop software.



Methods

Animals

Nine adult sika deer (Cervus nippon) stags of similar body weight (90–100 kg) were housed in an outdoor enclosure at DongAo Deer Farm for the duration of experimental procedures. Three were assigned for blood sample collection, and the other six were assigned to the wounding experiments. Experiments were performed during the period of rapid antler growth (June to August, ARP) and antler ossification (September to November, non-ARP). Male Sprague Dawley (SD) rats (weighing 150 g) were 6–8 weeks of age at the time of wounding. Rats were group housed (3 rats per cage) in a controlled environment (12 h light/dark cycle at 21–24 °C) with unrestricted access to water and a standard chow diet. Rats were randomly designated to each experimental group.

All manipulations on experimental deer and rats were performed under the guidelines and study protocols of the Institutional Animal Care and Use Committee of Changchun Sci-Tech University (Permit Number: CKARI202213, CKARI202321).

Skin wound creation and tissue collection

Sika deer wounding: three deer (stags 1, 2, and 3) were used during ARP and the other three (stags 4, 5, and 6) during non-ARP. All animal handling was done in the early morning to reduce any potential heat stress. The deer were

anesthetized (Medetomidine, 0.07-0.15 mg/kg) and then blindfolded. Sternal recumbency was maintained to reduce the risk of aspiration of regurgitated rumen contents. The depth of anesthesia, heart, and respiratory rate, and temperature were monitored continuously. Analgesia was accomplished with administration of a non-steroidal anti-inflammatory (Meloxicam, 0.5 mg/ kg). Forehead skin was clipped to remove hair and prepped with alternating betadine and alcohol wipes. One FTE wound (20 mm diameter) was created on the forehead skin of each deer. Sedation/anesthesia was then reversed (Atipamezole, intramuscular injection at 5 times the dose of medetomidine used). In each stag, each wound was sampled twice; healing tissue was collected from the wounds on stags 1 and 4 on day 3 post-operation (POD) and then allowed to heal before the second sample on day 30 POD; similarly, the wounds on stags 2 and 5 were sampled on day 9 and 60 POD, and those on stags 3 and 6, were sampled on day 14 and 60 POD. The healed tissues (harvested area: 0.3 cm² on day 3, 0.5 cm² on day 9, 0.6 cm² on day 14, 1.5 cm² on day 30 and 60) were harvested along the margin of the wounds by excisional biopsy utilizing the same anesthetic protocol.

SD rat wounding: all rats (n = 18 for ARPBP and non-ARPBP plus n = 9 for protein factors) were anesthetized with 2% isoflurane, their dorsal hair was removed with depilatory cream, and the exposed skin was sterilized with 70% ethanol and betadine. One round FTE wound was created for each rat with a sterile 12 mm biopsy punch on the dorsal skin between the

forelimbs and the hindlimbs. Each rat was housed in an individual cage after surgery. In rats receiving plasma, the procedure was: immediately following injury, 50 μ l of concentrated deer plasma (10x concentration) was injected subcutaneously into the uninjured tissue at the margin of each wound. The treatment was repeated weekly. At the indicated POD (3, 10, or 28, n=3 per time point), rats were euthanized by carbon dioxide inhalation, and the wound tissues were harvested by excising a 1.5 mm ring of tissue around each wound. For the protein factors used in rats per wound: 50 μ l of recombinant human IGF-1 (40 ng/ μ l; PeproTech, USA) or IGF-1/PRG4 (IGF-1: 2 μ g; recombinant human PRG4:0.5 μ g, CUSABIO, China); and the vehicle control, PBS, each was injected locally into the wound as described above. The treatment was repeated weekly. The wound tissues were collected on day 28 post-surgery (n=3).

All samples from deer wounds or rat wounds were divided into three parts. One-third of each sampled tissue was fixed in 4% paraformaldehyde immediately after removal. The next third was snap-frozen in clear optimum cutting temperature compound (OCT, Sakura, USA) on dry ice followed by storage at $-80\,^{\circ}\mathrm{C}$ until further use. The remaining third was flash-frozen in liquid nitrogen and stored at $-80\,^{\circ}\mathrm{C}$ until use.

After surgery, animals were monitored daily, and no aberrant behavior was detected.

Preparation of deer blood samples

Blood samples were collected from three male sika deer during the rapid antler regeneration phase (June, 2023) and again from the same deer during the antler ossification period in late autumn (October, 2023). All blood sample collections were carried out in the early morning (6:00 am) to minimize any heat stress. Deer were anesthetized as described above. Blood was drawn from the jugular vein and samples were collected in 0.1 M EDTA tubes. Plasma was obtained by centrifuging at 3000 rpm at 4 °C for 15 min, filtered through 0.22- μ m pore size filters (Millipore Corp, Billerica, MA), and stored at -80 °C. For animal experiments, plasma samples from the three deer were blended and further concentrated (10x concentration) via lyophilization, and finally rehydrated with PBS.

Histology

After fixation, the samples were washed with running water, dehydrated through serial ethanol washes, cleared with xylene, infiltrated with paraffin through serial incubations, and embedded in paraffin. Sections were cut at a thickness of 5 µm and incubated at 60 °C for 3 h to affix sections to slides prior to staining. Tissue sections were deparaffinized, rehydrated, and stained with haematoxylin-eosin (H&E) and Masson's trichrome using commercial kits (Solarbio, Beijing, China) according to the manufacturer's protocols. The stained images were captured under an inverted microscope (Nikon, Japan) or slice scanner (M8 microscope and scanner, PreciPoint, Germany).

Skin glands and extracellular matrix structure analysis

For evaluation of the density and architectural arrangement of collagen fibers, Picrosirius Red staining was performed using commercial kits (Tianenze, Beijing, China) according to the manufacturers' protocols. In brief, tissue sections were placed in Picrosirius Red solution for 2 h, washed and finally stained with hematoxylin for 5 min. Stained sections were dehydrated, mounted, and then imaged using polarized light microscope (Nikon, Japan).

Neogenic SGs were assessed and confirmed by Oil red staining using commercial kits (Beyotime, Shanghai, China) according to the manufacturers' protocols. In brief, frozen tissue was cryosectioned at 10 μ m thickness, and placed on positively charged slides. Tissue sections were thawed, washed with phosphate-buffered saline (PBS), and then placed in oil red staining solution for 20 min, washed and counterstained with haematoxylin for 5 min. After staining, tissue sections were photographed under a microscope (EVOS M5000, Thermo Fisher, USA).

Immunohistochemistry

For paraffin-embedded sections, immunohistochemistry was performed using an UltraSensitiveTM SP (Mouse/Rabbit) IHC Kit (MX

Biotechnologies, China) according to the manufacturer's protocol. Briefly, skin tissue sections were dewaxed, rehydrated with xylene and ethanol (100%, 95%, 80%, 70%), and subjected to antigen retrieval. Thereafter, the sections were washed in PBS, placed in 5% bovine serum albumin to block non-specific binding to antibodies, and then incubated with primary antibodies overnight at 4 °C. Sections were washed with PBS and incubated with biotinylated secondary antibody for 10 min at room temperature, visualized using DAB (3,3-diaminobenzidine) (MX Biotechnologies, China), and counterstained with haematoxylin for 5 min. Primary antibodies included rabbit anti-α-SMA (1:2000, Abcam, ab32575), rabbit anti-plastin-L (1:200, Abcam, ab109124), rabbit anti-ki67 (1:1000, Abcam, ab16667), rabbit anti-TGF-β3 (1:100, Abcam, ab15537), or mouse anti-TGF-β1 (1:100, Abcam, ab190503), rabbit anti-CD163 (1:500, Abcam, ab182422), rabbit anti-CD31 (1:1000, ab182981), rabbit anti-MPO (1:150, Abcam, ab9535). Images were captured under an inverted microscope (Nikon, Japan) or slice scanner (M8 microscope and scanner, PreciPoint, Germany). The number of Ki67⁺, CD163⁺, and MPO⁺ cells per field (2 fields per section, 3 sections) were counted manually. For the staining of plastin-L, α-SMA, TGF-β1, and TGFβ3, the MOD values per field (2 fields per section, 3 sections) were defined as IOD/area (the area indicated the total number of pixels in the picture) using Image-Pro Plus software. The ratio of TGF- β 3 to TGF- β 1 was calculated as the MOD mean value of TGF- β 3 to the MOD mean value of TGF- β 1.

For immunofluorescent staining, frozen tissues were cryosectioned at 10 μ m thickness, thawed, and then washed with PBS. Non-specific binding sites were blocked by incubating sections for 1 h in 10% goat serum containing 0.3% Triton-X in PBS. Primary antibodies were diluted in PBS and incubated overnight at 4 °C. The sections were washed three times with PBS and incubated with the secondary antibodies for one hour at room temperature; sections were washed with PBS for 3 min, and incubated with DAPI dye (1:500) for 5 min. Images were captured under a fluorescence microscope (EVOS M5000, Thermo Fisher, USA). The number of Ki67+ cells per field (2 fields per section, 3 sections) were counted manually.

Proteomic analysis

The differential protein expression of plasma samples collected in ARP and non-ARP was detected using DIA quantitative proteome technology by the Novegene Company (Beijing, China). In brief, total protein was extracted and quantified using the bicinchoninic acid assay (BCA assay), then digested with trypsin according to filter-aided sample preparation (FASP) protocol (Wisniewski et al.⁴⁷). The peptides obtained by FASP were desalted with C18-SD Extraction Disk Cartridge, and then dried via lyophilization and rehydrated with 40 µl of 0.1% formic acid. Purified digested peptide fractions were analyzed by LC-MS/MS using Orbitrap Astral high-resolution mass spectrometer. The LC-MS/MS raw files were uploaded into the DIA-NN software for database querying. The search parameters for the library were set with a mass tolerance of 10 ppm for precursor ions and 0.02 Da for fragment ions. Post-translational modifications encompassed alkylation of cysteine, oxidative modification of methionine, and N-terminal modifications such as acetylation, loss of methionine, and loss of methionine + acetylation. Furthermore, only one missed cleavage site was allowed. In this experiment, the identified proteins were defined by protein functional annotation, protein quantitative analysis, and differential protein expression analysis. Proteins were identified as differentially expressed (DEPs) if they demonstrated a |FoldChange| ≥ 1.5, with a p value <0.05. Using PANTHER 19.0⁴⁸, functional protein classification of the DEPs was further examined, focusing on the "Protein Class". KEGG pathway enrichment analysis was carried out by KOBAS-i⁴⁹. The mass spectrometry proteomics data have been deposited to the ProteomeXchange Consortium (https:// proteomecentral.proteomexchange.org) via the iProX partner repository^{50,51} with the dataset identifier PXD052882.

RNA sequencing

The healing skin tissues treated with plasma in ARP or non-ARP were used for RNA extraction. RNA-seq was performed by Gene Denovo Biotechnology Co. (Guangzhou, China), including RNA quantification, library

preparation, clustering, and sequencing. After removing low-quality reads (fastp 0.18.0)⁵², mapping to the Rattus norvegicus reference genome (Rnor_6.0, rn6) using HISAT2 2.1.0⁵³. An R package DESeq2⁵⁴ was used for DEGs examination, with a threshold absolute value of log2FC(Fold-Change) > 1 and FDR (false discovery rate) < 0.05. The raw matrix was further normalized to FPKM (fragment per kilobase of transcript per million mapped reads) for gene expression quantification. Subsequently, GO enrichment analysis and KEGG pathway enrichment analysis were performed using Omicsmart, a real-time interactive online platform for data analysis (http://www.omicsmart.com). Sequence reads were deposited in the NCBI Sequence Read Archive (SRA) under accession number PRINA1120002.

Establishment of cell co-culture system and tubing formation assay

The HUVEC cell line was from the cell bank in our lab (Jilin Provincial Key Laboratory of Antler Biology), and cultured in DMEM medium supplemented with 100 U/ml penicillin, 100 μ g/ml streptomycin, and 10% fetal bovine serum (HyClone, Beijing, China), in a humidified incubator with 5% (v/v) CO₂ atmosphere at 37 °C. For the establishment of cell co-culture assay, HUVECs were seeded at the bottom, and the DFCs or Raw264.7 cells were respectively seeded at the top using Transwell with 0.4 μ m inserts.

For tubing formation assay, 5×10^4 /well HUVECs of each group were seeded on the top of 100 µl matrigel (AWB, China) in a 48-well plate and incubated at 37 °C for 4 h. The pattern of tubing formation was stained using calcein and captured under a microscope (EVOS M5000, Thermo Fisher, USA). The tubing branch number and total branch length were analyzed by ImageJ software.

Statistical analysis

The results are presented as mean \pm SEMs. Statistical significance was evaluated using GraphPad Prism 9.0.1 (GraphPad Software, La Jolla, CA) software. The comparisons of single and multiple variables were performed using a one-way or two-way ANOVA, respectively, and Student's t test was used to compare two variables. Values were set at p < 0.05 for statistical significance.

Data availability

RNA sequence reads were deposited in the NCBI SRA under accession number PRJNA1120002. The mass spectrometry proteomics data have been deposited to the ProteomeXchange Consortium (https://proteomecentral.proteomexchange.org) via the iProX partner repository with the dataset identifier PXD052882. All data generated or analyzed during this study are included in this published article and its supplementary information files. Additional data are available from the corresponding author upon reasonable request.

Received: 13 August 2024; Accepted: 10 January 2025; Published online: 21 January 2025

References

- Mascharak, S. et al. Preventing engrailed-1 activation in fibroblasts yields wound regeneration without scarring. Science 372, eaba2374 (2021).
- Mascharak, S. et al. Multi-omic analysis reveals divergent molecular events in scarring and regenerative wound healing. *Cell. Stem Cell.* 29, 315–327 (2022).
- Sinha, S. et al. Fibroblast inflammatory priming determines regenerative versus fibrotic skin repair in reindeer. *Cell* 185, 4717–4736 (2022).
- Larson, B. J., Longaker, M. T. & Lorenz, H. P. Scarless fetal wound healing: a basic science review. *Plast. Reconstr. Surg.* 126, 1172–1180 (2010).
- Seifert, A. W. et al. Skin shedding and tissue regeneration in African spiny mice. *Nature* 489, 561–565 (2012).

- Zomer, H. D. & Trentin, A. G. Skin wound healing in humans and mice: challenges in translational research. J. Dermatol. Sci. 90, 3–12 (2018).
- Foster, D. S. et al. Integrated spatial multiomics reveals fibroblast fate during tissue repair. Proc. Natl Acad. Sci. USA 118, e2110025118 (2021).
- 8. Li, C., Yang, F. & Sheppard, A. Adult stem cells and mammalian epimorphic regeneration-insights from studying annual renewal of deer antlers. *Curr. Stem Cell Res. Ther.* **4**, 237–251 (2009).
- Li, C. & Chu, W. The regenerating antler blastema: the derivative of stem cells resident in a pedicle stump. Front. Biosci. 21, 455–467 (2016).
- Li, C., Suttie, J. M. & Clark, D. E. Morphological observation of antler regeneration in red deer (Cervus elaphus). J. Morphol. 262, 731–740 (2004).
- Guo, Q., Liu, Z., Zheng, J., Zhao, H. & Li, C. Substances for regenerative wound healing during antler renewal stimulated scar-less restoration of rat cutaneous wounds. *Cell Tissue Res.* 386, 99–116 (2021).
- Goss, R. J. Future directions in antler research. *Anat. Rec.* 241, 291–302 (1995).
- Kierdorf, U. et al. Histological studies of bone formation during pedicle restoration and early antler regeneration in roe deer and fallow deer. Anat. Rec. A Discov. Mol. Cell Evol. Biol. 273, 741–751 (2003).
- Li, C., Suttie, J. M. & Clark, D. E. Histological examination of antler regeneration in red deer (Cervus elaphus). *Anat. Rec. A Discov. Mol. Cell Evol. Biol.* 282, 163–174 (2005).
- 15. Li, C. Deer antler regeneration: a stem cell-based epimorphic process. Birth Defects Res. C. Embryo Today **96**, 51–62 (2012).
- Qin, T. et al. A population of stem cells with strong regenerative potential discovered in deer antlers. Science 379, 840–847 (2023).
- Guo, Q., Wang, D., Liu, Z. & Li, C. Effects of p21 gene down-regulation through RNAi on antler stem cells in vitro. *PLoS One* 10, e0134268 (2015), 26.
- Li, C. & Suttie, J. M. Histological studies of pedicle skin formation and its transformation to antler velvet in red deer (Cervus elaphus). *Anat. Rec.* 260, 62–71 (2000).
- Li, C. Exploration of the mechanism underlying neogenesis and regeneration of postnatal mammalian skin: deer antler velvet. *Int J. Med. Biol. Front.* 16, 1–9 (2010).
- Li, C., Mackintosh, C. G., Martin, S. K. & Clark, D. E. Identification of key tissue type for antler regeneration through pedicle periosteum deletion. *Cell Tissue Res.* 328, 65–75 (2007).
- Jaczewski, Z., Doboszyńska, T. & Krzywiński, A. The induction of antler growth by amputation of the pedicle in red deer (Cervus elaphus L.) males castrated before puberty. Folia Biol. 24, 299–307 (1976).
- Seifert, A. W., Monaghan, J. R., Voss, S. R. & Maden, M. Skin regeneration in adult axolotls: a blueprint for scar-free healing in vertebrates. *PLoS One* 7, e32875 (2012).
- 23. Pugliese, E., Coentro, J. Q., Raghunath, M. & Zeugolis, D. I. Wound healing and scar wars. *Adv. Drug Deliv. Rev.* **129**, 1–3 (2018).
- Reinke, J. M. & Sorg, H. Wound repair and regeneration. Eur. Surg. Res. 49, 35–43 (2012).
- Zhang, G. et al. Antler stem cell-derived exosomes promote regenerative wound healing via fbroblast-tomyofbroblast transition inhibition. J. Biol. Eng. 17, 67 (2023).
- Wang, Z. C. et al. The roles of inflammation in keloid and hypertrophic scars. Front. Immunol. 11, 603187 (2020).
- Buchanan, E. P., Longaker, M. T. & Lorenz, H. P. Fetal skin wound healing. Adv. Clin. Chem. 48, 137–161 (2009).
- 28. Schönborn, K. et al. Role of collagen XII in skin homeostasis and repair. *Matrix Biol.* **94**, 57–76 (2020).
- Amable, P. R. et al. Platelet-rich plasma preparation for regenerative medicine: optimization and quantification of cytokines and growth factors. Stem Cell Res. Ther. 4, 67 (2013).
- Estevez, B. & Du, X. New concepts and mechanisms of platelet activation signaling. *Physiology* 32, 162–177 (2017).
- Rong, X. et al. Transplanted antler stem cells stimulated regenerative healing of radiation-induced cutaneous wounds in rats. *Cell Transplant.* 29, 963689720951549 (2020).

- Rong, X. et al. Antler stem cell-conditioned medium stimulates regenerative wound healing in rats. Stem Cell Res. Ther. 10, 326 (2019).
- 33. Baron, J. M., Glatz, M. & Proksch, E. Optimal support of wound healing: new insights. *Dermatology* **236**, 593–600 (2020).
- Suttie, J. M. et al. Insulin-like growth factor 1 (IGF-1) antler-stimulating hormone? Endocrinology 116, 846–848 (1985).
- Bartos, L., Schams, D. & Bubenik, G. A. Testosterone, but not IGF-1, LH, prolactin or cortisol, may serve as antler-stimulating hormone in red deer stags (Cervus elaphus). *Bone* 44, 691–698 (2009).
- Park, J. et al. Study on the changes in enzyme and insulin-like growth factor-1 concentrations in blood serum and growth characteristics of velvet antler during the antler growth period in sika deer (Cervus nippon). Asian Australas. J. Anim. Sci. 28, 1303–1308 (2015).
- Suttie, J. M., Fennessy, P. F., Gluckman, P. D. & Corson, I. D. Elevated plasma IGF 1 levels in stags prevented from growing antlers. *Endocrinology* 122, 3005–3007 (1988).
- Sadighi, M., Haines, S. R., Skottner, A., Harris, A. J. & Suttie, J. M. Effects of insulin-like growth factor-I (IGF-I) and IGF-II on the growth of antler cells in vitro. *J. Endocrinol.* 143, 461–469 (1994).
- 39. Zhong, J. et al. Novel insights into the effect of deer IGF-1 on chondrocyte viability and IL-1beta-induced inflammation response. *J. Biochem. Mol. Toxicol.* **37**, e23227 (2023).
- Chablais, F. & Jazwinska, A. IGF signaling between blastema and wound epidermis is required for fn regeneration. *Development* 137, 871–879 (2010).
- Ikegawa, S., Sano, M., Koshizuka, Y. & Nakamura, Y. Isolation, characterization and mapping of the mouse and human PRG4 (proteoglycan 4) genes. Cytogenet. Cell Genet. 90, 291–297 (2000).
- Krawetz, R. J. et al. Proteoglycan 4 (PRG4) treatment enhances wound closure and tissue regeneration. NPJ Regen. Med. 7, 32 (2022). Jun 24.
- Ninkovic, N. et al. Proteoglycan 4 (PRG4) treatment improves skin wound healing in a porcine model. FASEB J. 38, e23547 (2024). 31.
- Walker, J. T., McLeod, K., Kim, S., Conway, S. J. & Hamilton, D. W. Periostin as a multifunctional modulator of the wound healing response. *Cell Tissue Res.* 365, 453–465 (2016).
- Shibata, S. et al. Adiponectin regulates cutaneous wound healing by promoting keratinocyte proliferation and migration via the ERK signaling pathway. *J. Immunol.* 189, 3231–3241 (2012).
- Feleke, M. et al. New physiological insights into the phenomena of deer antler: a unique model for skeletal tissue regeneration. *J. Orthop. Transl.* 27, 57–66 (2021).
- Wisniewski, J. R., Zougman, A., Nagaraj, N. & Mann, M. Universal sample preparation method for proteome analysis. *Nat. Methods* 6, 359–362 (2009).
- 48. Thomas, P. D. et al. PANTHER: Making genome-scale phylogenetics accessible to all. *Protein Sci.* **31**, 8–22 (2022).
- Bu, D. et al. KOBAS-i: intelligent prioritization and exploratory visualization of biological functions for gene enrichment analysis. *Nucleic Acids Res.* 49, W317–W325 (2021).
- Chen, K. et al. iProX: an integrated proteome resource. *Nucleic Acids Res.* 47, D1211–D1217 (2019).
- 51. Chen, T. et al. iProX in 2021: connecting proteomics data sharing with big data. *Nucleic Acids Res.* **50**, D1522–D1527 (2021).
- 52. Chen, S., Zhou, Y., Chen, Y. & Gu, J. fastp: an ultra-fast all-in-one FASTQ preprocessor. *Bioinformatics* **34**, i884–i890 (2018).
- 53. Kim, D., Langmead, B. & Salzberg, S. L. HISAT: a fast spliced aligner with low memory requirements. *Nat. Methods* **12**, 357 (2015).
- Love, M. I., Huber, W. & Anders, S. Moderated estimation of fold change and dispersion for RNA-seq data with DESeq2. *Genome Biol.* 15, 550 (2014).
- Crawford, J., Nygard, K., Gan, B. S. & Gorman, D. B. Periostin induces fibroblast proliferation and myofibroblast persistence in hypertrophic scarring. *Exp. Dermatol.* 24, 120–126 (2015).

- Zheng, Z. et al. Fibromodulin is essential for fetal-type scarless cutaneous wound healing. Am. J. Pathol. 186, 2824–2832 (2016).
- Zheng, Z. et al. Fibromodulin enhances angiogenesis during cutaneous wound healing. *Plast. Reconstr. Surg. Glob. Open* 2, e275 (2014).
- 58. Donovan, C. et al. Collagen XII regulates stromal wound closure. *Exp. Eye Res.* **230**, 109456 (2023).
- Zhu, X. L. et al. Adipokine adiponectin is a potential protector to human bronchial epithelial cell for regulating proliferation, wound repair and apoptosis: comparison with leptin and resistin. *Peptides* 40, 34–41 (2013).
- Liu, X. J. et al. Lumican accelerates wound healing by enhancing α2β1 integrin-mediated fibroblast contractility. PLoS One 8, e67124 (2013).
- 61. Yeh, J. T. et al. Impaired skin wound healing in lumican-null mice. *Br. J. Dermatol.* **163**, 1174–1180 (2010).
- Emmerson, E. et al. Insulin-like growth factor-1 promotes wound healing in estrogen-deprived mice: new insights into cutaneous IGF-1R/ERα cross talk. J. Invest. Dermatol. 132, 2838–2848 (2012).
- Botusan, I. R. et al. Vascular endothelial insulin/IGF-1 signaling controls skin wound vascularization. *Biochem. Biophys. Res.* Commun. 421, 197–202 (2012).
- 64. Tsuchida-Straeten, N. et al. Enhanced blood coagulation and fibrinolysis in mice lacking histidine-rich glycoprotein (HRG). *J. Thromb. Haemost.* **3**, 865–872 (2005).
- Klaas, M. et al. Thrombospondin-4 is a soluble dermal inflammatory signal that selectively promotes fibroblast migration and keratinocyte proliferation for skin regeneration and wound healing. *Front. Cell Dev. Biol.* 9, 745637 (2021).
- 66. Langan, E. A., Fink, T. & Paus, R. Is prolactin a negative neuroendocrine regulator of human skin re-epithelisation after wounding? *Arch. Dermatol. Res.* **310**, 833–841 (2018).

Acknowledgements

We would like to thank Dr. Peter Fennessy for critically reading through the manuscript. This work was supported by the National Natural Science Foundation of China (Grant Number: U23A20523; 32301151), the Development and Reform Commission of Jilin Province (Grant Number: 2023C040-9), the Science and Technology Development Plan Project of Jilin Province (Grant Numbers: YDZJ202201ZYTS435), the Doctoral Research Start-Up Fund of Changchun Sci-Tech University (Grant no. 202304), and the Chinese Key Natural Science Foundation (Regional Joint Funds; U20A20403).

Author contributions

Q.G. and C.L. conceived and designed the experiment. Q.G., G.Z., J.R., Z.W., J.L., Z.Y., and Y.W. performed the experiments. J.Z. and H.B. performed bioinformatics and statistical analyses. Q.G. and C.L. drafted and revised the manuscript. All authors read and approved the final manuscript.

Competing interests

The authors declare no competing interests.

Additional information

Supplementary information The online version contains supplementary material available at https://doi.org/10.1038/s41536-025-00391-5.

Correspondence and requests for materials should be addressed to Junjun Zheng or Chunyi Li.

Reprints and permissions information is available at http://www.nature.com/reprints

Publisher's note Springer Nature remains neutral with regard to jurisdictional claims in published maps and institutional affiliations.

Open Access This article is licensed under a Creative Commons Attribution-NonCommercial-NoDerivatives 4.0 International License, which permits any non-commercial use, sharing, distribution and reproduction in any medium or format, as long as you give appropriate credit to the original author(s) and the source, provide a link to the Creative Commons licence, and indicate if you modified the licensed material. You do not have permission under this licence to share adapted material derived from this article or parts of it. The images or other third party material in this article are included in the article's Creative Commons licence, unless indicated otherwise in a credit line to the material. If material is not included in the article's Creative Commons licence and your intended use is not permitted by statutory regulation or exceeds the permitted use, you will need to obtain permission directly from the copyright holder. To view a copy of this licence, visit http://creativecommons.org/licenses/by-nc-nd/4.0/.

© The Author(s) 2025